2. Mechanism and Upfault Seepage and Seismic Expression of Hydrocarbon Discharge Sites from the Timor Sea

Chapter · January 2013

DOI: 10.1190/1.9781560803119.ch2

CITATIONS
5

READS
565

7 authors, including:

Laurent Langhi
The Commonwealth Scientific and Industrial Research Organisation
57 PUBLICATIONS **357** CITATIONS
SEE PROFILE

Anthony Paul Gartrell
University of Western Australia
29 PUBLICATIONS **539** CITATIONS
SEE PROFILE

Jim Underschultz
The University of Queensland
164 PUBLICATIONS **1,633** CITATIONS
SEE PROFILE

David N. Dewhurst
The Commonwealth Scientific and Industrial Research Organisation
226 PUBLICATIONS **4,705** CITATIONS
SEE PROFILE

Chapter 2

Mechanism of Upfault Seepage and Seismic Expression of Hydrocarbon Discharge Sites from the Timor Sea

Laurent Langhi[1], Yanhua Zhang[1], Anthony Gartrell[2], Mark P. Brincat[3], Mark Lisk[4], Jim Underschultz[5], and David Dewhurst[1]

Abstract

Three-dimensional coupled deformation and fluid-flow numerical modeling, charge-history analysis, and seismic imaging of inferred leakage-related geobodies are integrated to investigate the response of a complex set of Jurassic trap-bounding normal faults to extensional reactivation and to assess hydrocarbon upfault seepage on the Laminaria High (Timor Sea, Australian North West Shelf). Fluid inclusion data are consistent with the presence of paleo-oil columns below the current accumulations in the Laminaria and Corallina fields. Evidence for other partially breached (current and paleo-oil column) as well as breached (dry with paleo-oil column) closures across the region implies that active and widespread seepage took place after the time of initial oil charge. The distribution of current and paleo-oil zones, and the location of inferred hydrocarbon leakage indicators defined on 3D seismic data, correlates with the prediction of fault-seal effectiveness based on modeled strain distribution. Within the geologic framework of the Laminaria High area, this distribution suggests that when sufficient reactivation shear strain is accumulated by reservoir faults, ductile deformation might give way to brittle failure in the top seal, allowing active flow pathways to develop and upfault seepage to take place from the reservoir to thief zones or the seafloor. The observations emphasize that strain and upfault fluid-flow partitioning is constrained by prereactivation fault size, lateral fault-tip distributions, and the presence of fault jogs inherited from successive episodes of growth processes. These elements can explain the complex distribution of paleo- and preserved oil columns in the study area and further support Cenozoic tectonic activity as being the first-order control on trap breaching and hydrocarbon seepage in this region.

Introduction

Faults can be conduits or barriers to fluid flow, depending on stress conditions, strain distribution, tectonic settings, and rock properties and distribution (Bjørlykke et al., 2005). Although permeability across faults may obviously result in fewer fault traps and perhaps less reservoir compartmentalization and column height, crossfault migration may be important during field production. Permeability along faults has an important role as a hydrocarbon migration route from source rocks and plays a role in overpressure development and/or upfault leakage (e.g., Fisher and Knipe, 2001; Fisher et al., 2003; Færseth et al., 2007; Underschultz, 2007). Critically stressed faults (e.g., reactivated faults) are widely cited as conduits for fluid flow (Anderson et al., 1994; O'Brien et al., 1999; Revil and Cathles, 2002; Ligtenberg, 2005).

[1]*CSIRO (Commonwealth Scientific and Industrial Research Organization), Earth Science and Resource Engineering, Australian Resource Research Centre (ARRC), Perth, Australia. E-mail: laurent.langhi@csiro.au; yanhua.zhang@csiro.au; david.dewhurst@csiro.au.*

[2]*Shell Australia Ltd., Perth, Australia. E-mail: gartrell.anthony@gmail.com.*

[3]*INPEX, Perth, Australia. E-mail: mark.brincat@inpex.com.au.*

[4]*Woodside Energy Pty Ltd., Perth, Australia. E-mail: mark.lisk@woodside.com.au.*

[5]*Formerly CSIRO, Perth, Australia. Presently Australian National Low Emissions Coal R&D (ANLEC), Manuka, Australia. E-mail: james.underschultz@anlecrd.com.au.*

The mechanisms by which fault reactivation results in the leakage of hydrocarbons are not well understood (e.g., Revil and Cathles, 2002; Wilkins and Naruk, 2007). However, the relationship between tectonic activity and leakage is not under debate (e.g., Muir-Wood and King, 1993; Haney et al., 2005), and active faulting in the brittle upper crust is associated with the generation of dilatant strains and consequently increased porosity and permeability. Whether leakage occurs as a consequence of buildup and release of geopressured fluids (e.g., Sibson, 1992, 1996; Sleep and Blanpied, 1992), as a result of critical stressing of faults (Barton et al., 1995), or because of slip-induced dilation (Wilkins and Naruk, 2007) is uncertain; but documentation of fluid flow in seismically active basins demonstrates a clear link between active faulting and vertical fluid flow in permeable conduits (e.g., Anderson et al., 1994; Losh, 1998; Losh et al., 1999; O'Brien et al., 1999; Revil and Cathles, 2002; Heggland, 2005; Ligtenberg, 2005; Underschultz et al., 2005).

The exploration risk associated with late-stage fault-seal breach is recognized as a major issue affecting hydrocarbon prospectivity in the Timor Sea (Bonaparte Basin, Australian North West Shelf; Figure 1). The high incidence of breached or underfilled Jurassic hydrocarbon traps is commonly considered to result from Neogene extensional to transtensional tectonic reactivation affecting most of the trap-bounding faults (O'Brien et al., 1996; Shuster et al., 1998; O'Brien et al., 1999; Gartrell and Lisk, 2005; Gartrell et al., 2006; Rollet et al., 2006). *Prima facie* evidence for this outcome is provided by the abundant reactivated faults that regularly pierce the seal; however, not all of these faults appear to result in upfault

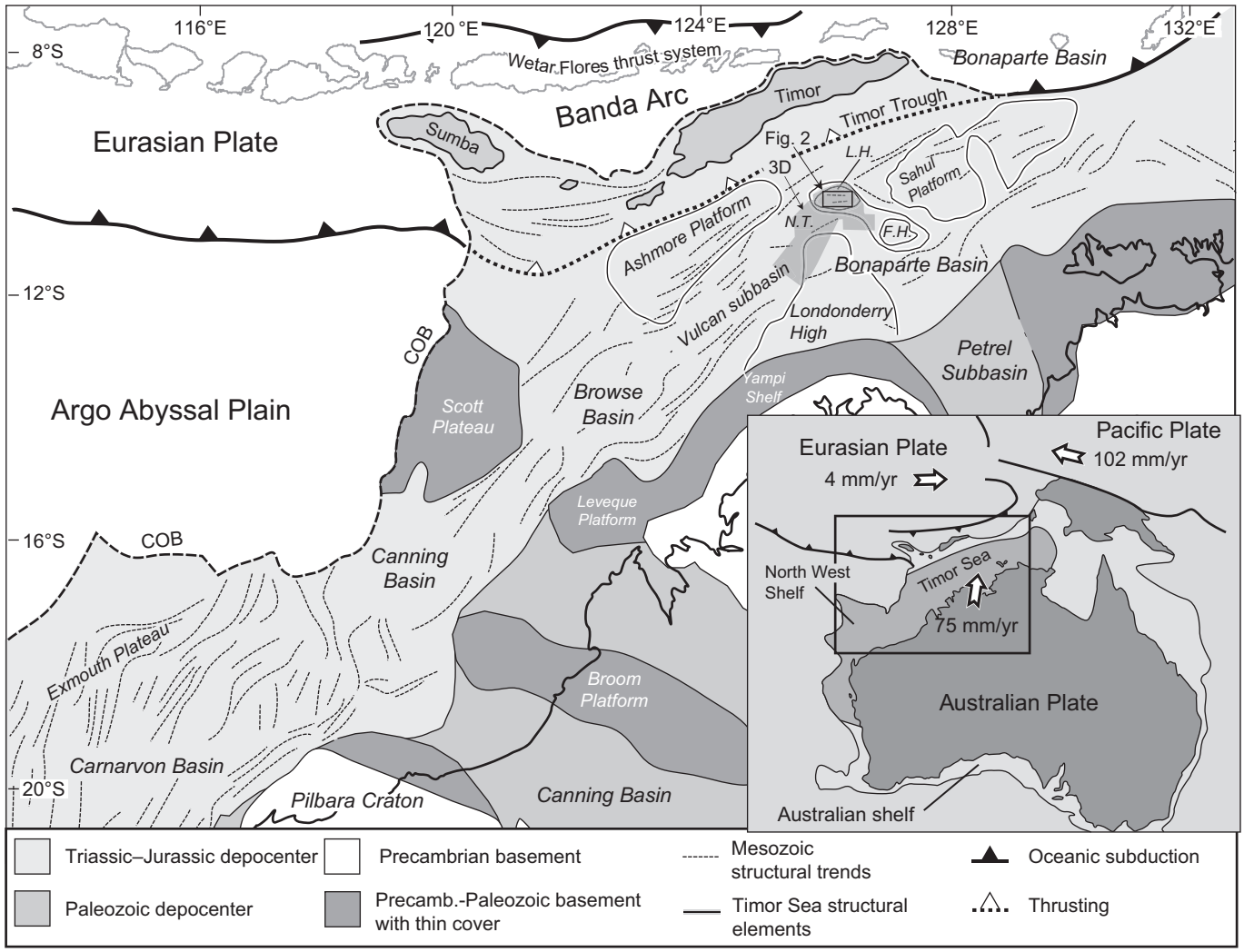

Figure 1. Geologic elements of the North West Shelf and the Bonaparte Basin, modified after AGSO (1994) and Harrowfield et al. (2003): COB = continent ocean boundary, L.H. = Laminaria High, N.T. = Nancar Trough, F.H. = Flamingo High, 3D = northern Vulcan megasurvey MC3D.

hydrocarbon leakage. Therefore, the accurate prediction and characterization of along-fault hydrocarbon remigration pathways is a critical element in the effective risking of exploration traps as well as being an important implication for production well design.

Numerical geomechanical models have been applied in the region to minimize geologic risks due to fault reactivation and to simulate more specifically the behavior of faults and fluids in response to reactivation. Zhang et al. (2009) characterize the interaction between stress and strain states and the development of fluid-flow conduits based on the response of simplified faults and reservoir-seal geometries to extensional reactivation. Langhi et al. (2010) construct a complex coupled deformation and fluid-flow numerical model for the Laminaria High (Bonaparte Basin, Timor Sea, Australian North West Shelf), highlighting the heterogeneous distribution of shear strain and dilation as well as fluid flux.

This chapter aims to further test the numerical modeling approach through more sophisticated geomechanical modeling constrained by additional empirical observations to investigate hydrocarbon preservation risk for complex reactivated structural traps in the Laminaria High area. Based on the integration of independent data on (1) charge history from fluid inclusion analysis and (2) fluid upfault leakage from 3D seismic interpretation and attribute mapping, we investigate and calibrate key structural elements impacting upfault fluid-flow and trigger mechanisms, and we propose a conceptual model identifying preferential remigration pathways and discharge processes.

Geologic framework and petroleum system

The area of study covers the Laminaria High in the northern Bonaparte Basin, a Mesozoic-Cenozoic depocenter on the northern part of the Australian North West Shelf (Figure 1). The preexisting Paleozoic structural grains, including Late Devonian to Early Carboniferous northwest-trending extensive structures and Permo-Carboniferous northeast–southwest rift-related structures, are generally too deep to be observed on seismic data but could have locally significant influence on the distribution and thickness of the Mesozoic-Cenozoic deposits (de Ruig et al., 2000).

Successive episodes of rifting that culminate with Late Jurassic–Early Cretaceous rifting associated with the opening of the abyssal plains (AGSO, 1994; Baillie et al., 1994) are responsible for the development of the Mesozoic structural trend in the Bonaparte Basin. The associated southwest–northeast strike generally observed in the Bonaparte Basin and on the North West Shelf (Figure 1) changes to east–west in the Nancar Trough and Laminaria High area (Figure 2; see de Ruig et al. [2000] and Langhi and Borel [2008]). The resulting structural architecture in this area is characterized by horst-and-graben systems and fault blocks typical of a rifted margin, with abundant steeply dipping normal faults (40°–60°). Structural mapping at the Jurassic level shows fault strike lengths ranging from approximately 1 to 30 km (~0.6–18.6 miles), with the smallest structures usually representing simple linear fault zones and the longer ones displaying jogs resulting from lateral fault growth processes and segment linkage (Figure 2; see Marchal et al. [2003] and Langhi and Borel [2008]).

The local stratigraphic succession (Figure 3) clearly records the rifting and subsequent postrift subsidence with (1) the early synrift Plover and Laminaria deltaic and shallow marine formations (Labutis et al., 1998), (2) the Late Jurassic to Cretaceous shale (Frigate, Flamingo, and Echuca Shoals Formations) from the deepening continental shelf (Whittam et al., 1996), and (3) the Aptian–Maastrichtian interval of stacked progradational wedges (Darwin, Jamieson, Woolaston, Gibson, Fenelon, and Turnstone Formations) comprised of silty claystones cleaning up to calcareous shale and marl-prone sediments (Whittam et al., 1996). From the late Mesozoic through most of the Cenozoic era, the Timor Sea represented a mature passive margin characterized by an extensive cover of prograding shelf carbonates (Johnson, Hibernia, Prion, Cartier, Oliver, and Barracouta Formations) (Whittam et al., 1996).

From at least the Miocene onward, the geologic evolution of the area has been influenced increasingly by the complex oblique collision between the Australian plate and the Southeast Asia plate, resulting in the accretion of the Timor prism (Figure 1) (O'Brien et al., 1993) and the development of an underfilled foreland basin that includes the Bonaparte Basin (Figure 1). The resulting lithospheric flexure due to thrust loading at Timor Island is believed to generate a widespread but relatively small amount of postrift extensional reactivation observed in the region (Bradley and Kidd, 1991; Lorenzo et al., 1998; Langhi et al., 2011). The onset of the collision between the Australian continental crust and the Banda volcanic arc is dated to the Late Miocene from about 8 million years ago (Ma) (e.g., Shuster et al., 1998; Charlton, 2000; Keep et al., 2002) (Figure 3), with fault activity occurring at the Miocene-Pliocene boundary and during the Pliocene (Charlton et al., 1991; O'Brien et al., 1999). This fault activity resulted in the formation of sets of east-northeast–west-southwest-trending normal faults within the Cenozoic cover sequence in the study area, usually clustering above the preexisting rift faults.

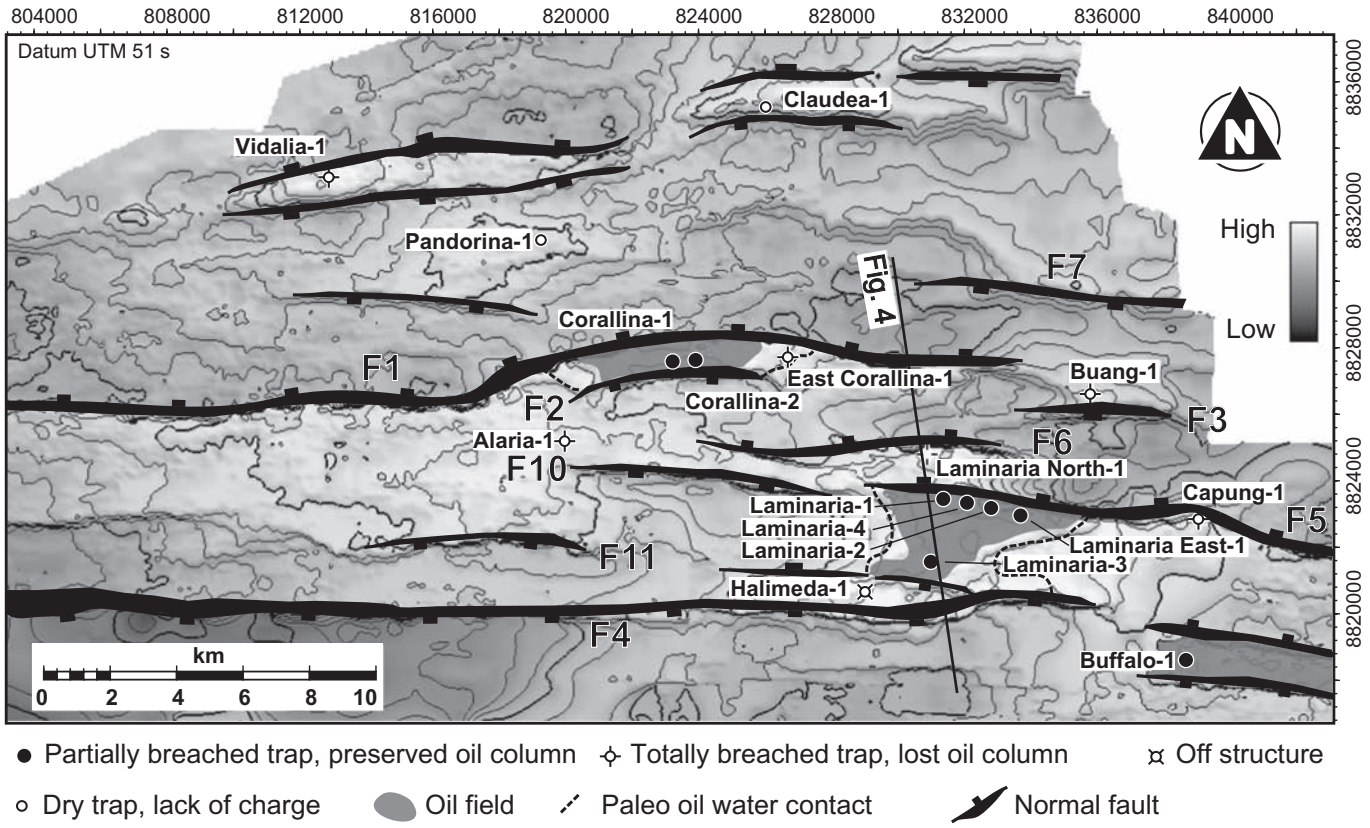

Figure 2. Base Oxfordian sandstone (reservoir) time-structure map and distribution of the wells and oil fields for the Laminaria High. Location is on Figure 1.

The connection between fault traces at Jurassic and Cenozoic levels (Figure 4) is sometimes difficult to ascertain because of the nature of intervening Cretaceous lithology (shale, mudstone, and marl), seismic signal degradation, and subseismic faulting (Gartrell et al., 2006). However, faults with higher postrift displacements tend to show clearer connectivity between the Upper Cenozoic and Lower Jurassic levels.

The petroleum system of the region has been well described (e.g., Lisk et al., 1998; Kennard et al., 1999; Longley et al., 2002), with all of the components needed to form hydrocarbon accumulations. Traps are abundant, principally as tilted fault blocks or narrow horst-block structures. The Callovian-aged Laminaria Formation (Figure 3) was deposited as synrift, mostly shallow marine sediments that infill accommodation space created by Jurassic tilted normal fault blocks. These blocks constitute the dominant exploration target in the northern Bonaparte Basin. Source-rock intervals are found in the Jurassic Plover and Laminaria Formations. There is ubiquitous evidence for hydrocarbon charge in the northern Bonaparte study area in terms of the current fields as well as oil-filled fluid inclusions (Lisk and Eadington, 1994; Brincat et al., 2001). Conventional shows and leakage indicators (O'Brien and Woods, 1995; O'Brien et al., 1996) provide overwhelming support that most traps accessed charge. The main phase of oil charge is interpreted near the Middle Eocene (about 50 Ma; Kennard et al., 1999). Across the region, an initial Late Jurassic–Early Cretaceous gas charge, followed by widespread late-stage gas and oil charges from the Miocene onward, has been proposed (Lisk et al., 1998; Kennard et al., 1999).

The thick, ductile, regionally extensive Early Cretaceous marine mudstone and shale (Figure 3) form the effective regional top and lateral seals to these traps. On the Laminaria High, at no point is the seal offset by faulting; closures are always located within fault juxtaposition seal limits. Therefore, cross-fault leakage due to the juxtaposition of sandstone units is not anticipated. Top-seal failure risk is low, based on (1) the high predicted membrane seal quality (oil-column heights of 150–400 m; de Ruig et al. [2000] and references therein), (2) the absence of thief zones in the top seal (de Ruig et al., 2000; W. Bailey, personal communication, 2009), and (3) the absence of present-day aquifer overpressures.

However, the trap architecture has been reactivated during late Tertiary to recent convergence between the Eurasian and Australian plates (Figure 1). The resulting shear

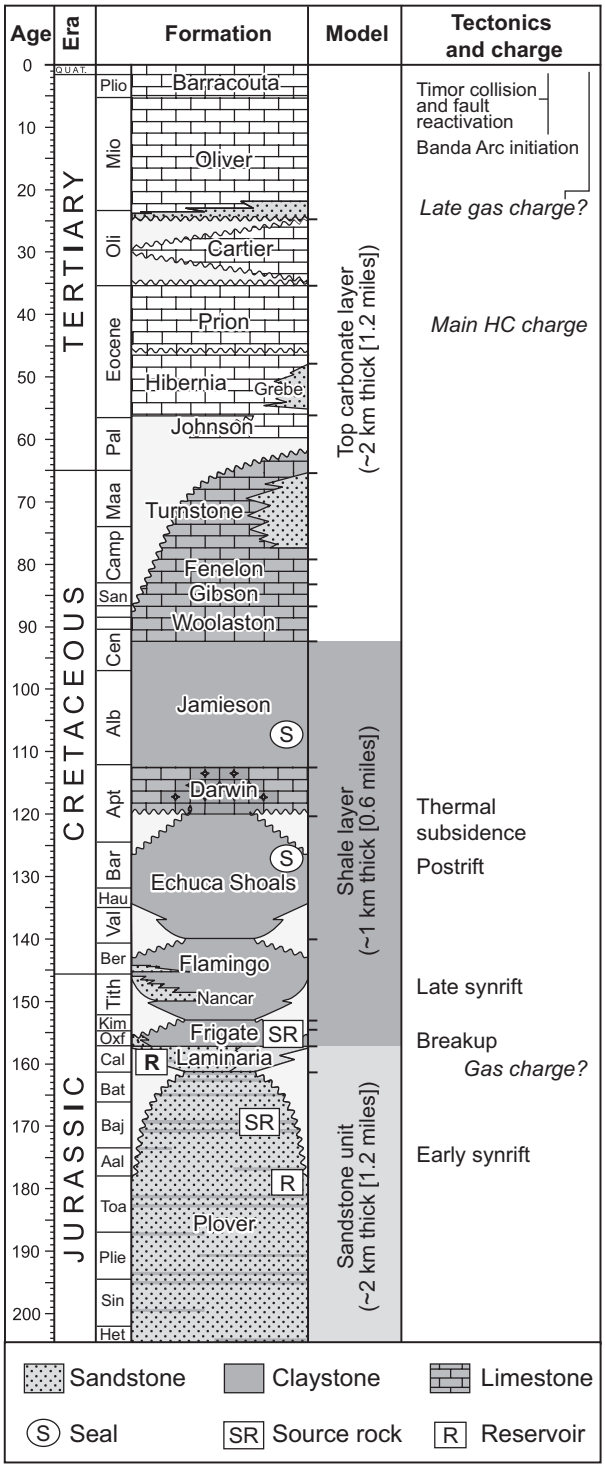

Figure 3. Schematic stratigraphic column for the Laminaria High area, modified from de Ruig et al. (2000). The model column shows the subdivision used in the numerical modeling. HC = hydrocarbon.

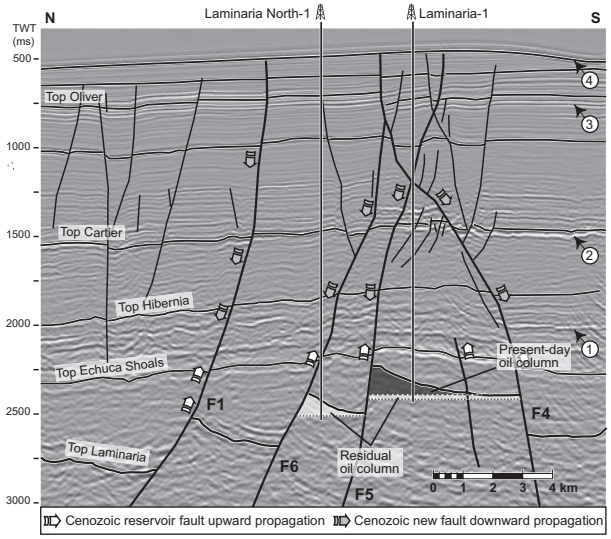

Figure 4. Typical cross section across the Laminaria High; location is on Figure 2. ① Grebe sandstone thief zone (?), ② Oliver basal member thief zone, ③ Miocene-Pliocene expulsion site, ④ present-day seabed expulsion site. Laminaria North is breached and has lost all hydrocarbons; Laminaria, also breached, lost only a small amount of reservoired hydrocarbons. F1, F4, F5, and F6 refer to faults on Figure 2.

failure associated with fault reactivation is considered to be the mechanism responsible for trap breaching in the Laminaria High area and the Timor Sea (Castillo et al., 1998; O'Brien et al., 1999; Gartrell et al., 2006). A paper by de Ruig et al. (2000) rules out seal failure occurring from tensile or hydraulic fracturing due to high differential stresses that favor shear fracturing and reactivation of existing faults over hydraulic fracturing as pore pressures rise.

Severe changes in trap geometry (e.g., tilting) that could cause hydrocarbons to be lost from closures are not postulated because the gross fault-block organization was established during Jurassic rifting. Water washing has also been proposed as an alternative mechanism to explain the significant underfilling of the traps in the study area (Newell, 1999), but data from George et al. (2004) suggest that this model is unlikely to represent a first-order control on the degree of current trap fill. Most published works (e.g., O'Brien et al., 1996; Shuster et al., 1998; O'Brien et al., 1999; Gartrell and Lisk, 2005; Gartrell et al., 2006) consider the vertical remigration of hydrocarbons along Tertiary reactivated fault planes as the most likely explanation for trap breach.

Data and methodology

Data

Our study is based on the interpretation of 3D seismic-survey and well data covering the Laminaria High and extending to the Nancar Trough (Figure 1). The structural and

stratigraphic mapping relies on the interpretation of the northern part of the Vulcan subbasin MC3D megasurvey (Edwards et al., 2005), provided by PGS Exploration, Australia. This data set is comprised of five separate surveys acquired between 1995 and 1999, merged into an integrated 3D migrated volume in 2000. The raw DMO stacks of each survey were merged and output as three volumes: a raw DMO stack volume, a raw migration volume, and a final filtered migration volume with SEG negative polarity which is used in this study. The 3D seismic data cover approximately 5600 km^2 (~2160 $miles^2$) over the Laminaria High, Nancar Trough, and Londonderry High. The grid is oriented to the northeast, with final symmetric bin spacing of 56×56 m (184×184 ft).

A representative cross section from the study area shows that the Cenozoic carbonate section is characterized by a high signal-to-noise ratio (S/N) (Figure 4). The high S/N decreases in the Early Cretaceous–Late Jurassic section as a result of the presence of low reflectivity at the top of the reservoir (Smith et al., 1996). This reduction in S/N has contributed to poor imaging of the top of the porosity level and has adversely impacted accurate trap definition.

Eighteen closures have been drilled within the study area, with a total of 40 vertical and deviated wells. They provide standard petrophysical and lithological data used in interpretation and static model building as well as samples for the fluid-inclusion analyses used to assess basic charge history of Late Jurassic reservoirs and paleoaccumulations.

Hydrocarbon charge history

Initial indications of hydrocarbon charge usually come from conventional oil shows in the form of fluorescence and mud-gas levels measured during drilling. The intensity of these shows is often used to infer the presence of an intact or residual oil column, but these shows can be degraded by the drilling process — particularly in lightly explored basins where wells are often drilled overbalanced to counter unexpected drilling kicks.

Conventional oil and gas shows can be combined with unconventional oil and gas shows provided by oil-bearing fluid inclusions to investigate hydrocarbon-fluid contacts and to provide a more comprehensive evaluation of the oil-charge history and oil-migration risks in petroleum reservoirs (e.g., Karlsen et al., 1993; Lisk and Eadington, 1994; Isaksen et al., 1998; Lisk et al., 1998, 2001; Brincat et al., 2001; Gartrell and Lisk, 2005; Brincat et al., 2006).

These unconventional oil-show methodologies rely on detecting small samples of migrating hydrocarbons that become entrained within the rocks and sealed as fluid inclusions from the pore volume during cementation. Fluid inclusions are protected from contamination introduced while drilling and are not affected by time or conditions of sample storage, making them ideal for retrospective analysis.

Fluid inclusions are microscopic (commonly 2–50 μm) samples of paleopore-space fluids that form during burial processes and are encapsulated within suitable host minerals. Suitable host materials are commonly comprised of fractured detrital quartz or feldspar grains, their authigenic overgrowths, or any pore-filling cement with a framework crystal structure. Fluid inclusions can occur within time-specific diagenetic cements, usually once the reservoir temperatures exceed 80°–90°C or about 2200 m (e.g., Worden and Morad, 2000). Alternatively, inclusions may be trapped along healed fractures within the detrital grains, formed throughout most of the burial history. Fluid inclusions may contain varying percentages of gas, oil, and water and may be thought of as proxy sample points of pristine pore-space fluid at the time the inclusion was sealed off from the pore network.

GOI™ technique

The grains with oil inclusions (GOI™) technique (Lisk and Eadington, 1994; Eadington et al., 1996) is used to assess the frequency of oil inclusions and to assess the level of paleo-oil saturation (e.g., Lisk et al., 2001; Lisk et al., 2002; Brincat et al., 2006). GOI numbers represent the percentage of quartz and feldspar grains containing oil-bearing fluid inclusions in sandstone that are compared against an empirical database of GOI values from known oil fields to estimate the maximum oil saturation of a reservoir through time (Eadington et al., 1996; Lisk et al., 1998).

- GOI values less than 1% indicate samples that show no evidence of high oil saturation.
- GOI values greater than 5% are used to infer attainment of high oil saturation *So* (>30% or formation of an oil column) at some time.
- The positions of paleo-oil/water contacts (paleo-OWCs) are defined by a significant and sustained drop in GOI values, typically to values of less than 1%.

Unlike conventional oil shows, oil trapped within fluid inclusions is sealed from the pore network and is impervious to changes in fluid type caused by leakage, water washing, and gas flushing; the oil is not altered by contamination introduced during drilling.

Limitation

The fluid-inclusion trapping process may be hindered by circumstances other than reservoir quality. The presence of ductile minerals such as glauconite can cushion the

detrital quartz grains and hinder the ability of these grains to fracture. This condition prevents oil inclusions from being trapped when these fractures are recemented by local pressure solution effects. Glauconitic content greater than 5% will reduce the order-of-magnitude variation among the samples that have always had low oil saturation and those samples that had high oil saturation sometime in the past (Lisk et al., 1996). Fracturing of quartz grains also relies on depth, and this process appears to initiate at depths exceeding 1000 m; so GOI samples taken from depths shallower than 1000 m are more likely to produce a false negative and therefore have lower confidence.

Coupled geomechanical deformation and fluid-flow modeling

The FLAC3D (fast Lagrangian analysis of continua 3D) finite-difference code is used in this study to simulate the interactions between deformation and fluid flow in rocks (Cundall and Board, 1988; Itasca, 2005). A brief description is provided here; readers are referred to Itasca (2005), Ord (1991), Ord and Oliver (1997), Strayer et al. (2001), and McLellan et al. (2004) for detailed descriptions of the constitutive laws governing deformation and fluid flow in the code.

In the simulations, rock materials and geometries (i.e., stratigraphic layers and fault zones) are represented by hexahedral elements forming a 3D continuum mesh and are simulated as Mohr-Coulomb isotropic elastic-plastic materials fully coupled with fluid flow (Cundall and Board, 1988; Itasca, 2005; see also Vermeer and de Borst [1984], Ord [1991], and Strayer et al. [2001]). They behave according to the Mohr-Coulomb isotropic elastic-plastic constitutive law for mechanical deformation and Darcy's law for fluid flow in response to the applied boundary conditions. As such, the modeled material deforms initially in an elastic manner until the maximum shear stress reaches the yield threshold magnitude τ_s and then deforms plastically to large irreversible strain after yielding. The Mohr-Coulomb yielding criteria are described by

$$|\tau_s| = C - \sigma_n \tan\varphi, \tag{1}$$

where τ_s is the yield threshold shear stress, C is the cohesion, σ_n is the normal stress on an arbitrary plane in the material, and φ is the friction angle.

The postyielding plastic strain is governed by a nonassociated plastic-flow law with constant cohesion C, friction φ, and dilation angles ψ (Vermeer and de Borst, 1984). During plastic shearing deformation, a Mohr-Coulomb material may undergo positive volume strain (i.e., volume increase or dilation) (Ord and Oliver, 1997). The dilatant potential of the Mohr-Coulomb material for plastic deformation is characterized by a positive dilation angle ψ. Additional parameters for the mechanical deformation include shear modulus G, bulk modulus K, and tensile strength T. These parameters are kept constant during a simulation.

Fluid flow (single phase) is coupled with mechanical deformation during a simulation and is governed by Darcy's law for an isotropic porous medium (Bear and Verruijt, 1987). It involves the permeability tensor k_{ij} (in m^2), fluid viscosity μ, pore-fluid pressure P, fluid density ρ_w, acceleration g, position of the sample points x_j and y_i, and elevation z. The calculated Darcy fluid-flow velocities V_{ij} are primarily a function of gradients in pore-fluid pressures and variations in permeability, given by

$$V_{ij} = -(k_{ij}/\mu)\, \partial/\partial x_j\, (P - \rho_w g\, z). \tag{2}$$

Four main aspects characterize the interaction between mechanical deformation and fluid flow. First, deformation-induced volumetric strains or mechanical volume changes cause fluid pore-pressure changes (e.g., a local dilation will lead to a local pore-pressure decrease). Second, changes in fluid pore pressure result in changes in the effective stress in modeled rocks and hence affect material yielding (e.g., a local reduction in effective stress will facilitate plastic yield). Third, the development of any topographic features resulting from bulk deformation will lead to changes in fluid-flow patterns by affecting pore pressure and/or head distribution. Fourth, mechanical deformation could lead to permeability enhancement and hence change fluid-flow patterns (see "Fault Permeability Variation Scheme" and "Discussion," following).

Limitation

The modeling methodology of this study relies on a Mohr-Coulomb elastic-plastic constitutive law that incorporates a constant, small dilation angle. Thus, a fault subjected to reactivation shearing will dilate constantly with the accumulation of shear strain. Such behavior is reasonable for the low-to-intermediate degrees of fault reactivation shearing, which is the case in our study. But it could lead to overestimating dilation in highly sheared faults, on which the development of dilatancy could diminish due to fault-gouge development. Similarly, the simple permeability enhancement scheme of this study only applies to faults with low-to-intermediate degrees of reactivation and shearing, where fracture-damage permeability enhancement dominates (Caine et al., 1996), rather than to highly sheared faults with well-developed fault-gouge materials.

The outcome of the coupled modeling is highly dependent on the applied boundary conditions. For our study, the stress regime represents a regional estimate, constrained by a paleostress inversion produced in the Timor Sea (Gartrell and Lisk, 2005); the bulk extension is consistent with regional knowledge (e.g., Longley et al., 2002; Gartrell and Lisk, 2005; Gartrell et al., 2006). Although local variations might occur, such conditions should reasonably capture the Cenozoic tectonic regime. The initial pore-pressure condition used in the modeling is locally constrained by in situ pressure data. However, it still represents a simplified scenario, and this parameter can affect the local fluid flow and the distribution of stresses and strains. The modeling of fluid flow is strongly dependent on the simplistic fault permeability variation scheme proposed here. We acknowledge that this approach does not take into account the full complexity of the permeability distribution and the evolution in a fault zone; however, we postulate that it can be used for first-order qualitative tests of our proposed geologic model.

Seismic mapping

Fluid migration (including hydrocarbons) resulting from upfault leakage will most likely affect the morphology (e.g., Hovland and Judd, 1988; Hovland et al., 1994; Ligtenberg, 2005) and bulk proprieties of a rock body (Judd et al., 1992) in or around fault zones and within adjacent discharge sites. The various seismic attributes and mapping/analysis techniques presented in the following sections have been combined to image and characterize the remigration system from the Jurassic reservoirs to the overburden or free surface in the study area.

Discharge sites

In the Timor Sea, hydrocarbon leakage defined on seismic data has been inferred from hydrocarbon-related diagenetic zones (HRDZs), which produce acoustic anomalies and a pull-up effect following remigration of hydrocarbon in shallow aquifers and the resulting cementation process (e.g., O'Brien and Woods, 1995; Cowley and O'Brien, 2000). Specific environmental conditions needed to promote the formation of HRDZs could explain the absence of HRDZs in the study area; instead, buried thief zones and expulsion sites fed by conductive structures are believed to represent the main seismically mapped indications of vertical hydrocarbon leakage (Figure 4). Local amplitude anomalies are the most common seismic expression of such inferred discharge sites. Bright spots are expected in porous sandstones that are intercalated within the carbonate-dominated Tertiary section that contains residual hydrocarbons as well as shallow sediments presently containing gas (e.g., Heggland, 2005; Ligtenberg, 2005; Roberts et al., 2006; Rollet et al., 2006; Halliday et al., 2008).

Authigenic carbonate hardgrounds and localized carbonate reef development, potentially resulting from hydrocarbon leakage (e.g., Hovland et al., 1994; Bailey et al., 2003; Roberts et al., 2006), can also produce restricted zones of high-reflectivity seismic facies.

More than a dozen common attributes capture the variation of seismic reflectivity (e.g., reflection strength, rms amplitude, true amplitude, energy), although most of them are strongly correlated to one another and all display the same basic information (Barnes, 2007). In this study, we frequently use the energy attribute returning the squared sum of the sample values in a specified time window. Spectral decomposition has also been used to further quantify the reflectivity in volumes of interest and to investigate features that tune at a given frequency rather than at the dominant frequency of the source wavelet. This practice allows for a thorough assessment of the lateral variation of geobodies (e.g., Partyka et al., 1999; Giroldi et al., 2005). Additional attributes such as similarity, dominant frequency, dip, azimuth, and curvature have also been used to discriminate discharge sites on the basis of their continuity, frequency content, and geometry.

Near-fault remigration pathways

Faults acting as conduits for fluids from Jurassic reservoirs might be associated with low-energy and chaotic near-vertical seismic facies that are interpreted as hydrocarbon chimneys (e.g., Ligtenberg, 2005).

In an attempt to further assess the distribution of active remigration pathways in the study area, a meta-attribute chimney cube (Meldahl et al., 2001; Aminzadeh et al., 2002; Ligtenberg, 2003) has been computed. Standard 3D seismic data and a set of attributes capturing the reflectivity, similarity, frequency, and dip of the seismic signal are integrated with training data defined by the interpreter and inferred to represent fault-related leakage features. These data are then used to train a neural network. Transparent and chaotic vertical seismic zones can be caused by factors other than hydrocarbon migration, so the chimney cube requires validation against additional information such as discharge sites seen in seismic data and coupled modeling outputs.

Limitation

An important factor limiting the seismic imaging of leakage geobodies is the lack of well control. Indications of

leakage presented here are not calibrated by wells; therefore, their interpretation relies on crosscorrelation with independent elements such as (1) estimation of the most likely seismic response to changes of bulk proprieties caused by hydrocarbon leakage, (2) the similarity with published and well-documented seismic leakage indicators (e.g., Heggland, 2005; Ligtenberg, 2005; Roberts et al., 2006; Rollet et al., 2006; Halliday et al., 2008), and (3) the relationship with the local structural network and the distribution of breached or underfilled closures. Where hydrocarbon chimneys have been interpreted, away from the shadow effect of faults and shoals, they are delimited by a main leaking fault plane and antithetic and synthetic faults. This structural framework could create some of the incoherency usually associated with chimneys on seismic data. However, we estimate that this secondary faulting can also enhance the structural permeability in the vicinity of the main fault plane and trigger or sustain the development of a pathway next to the plane.

Charge history and fluid-inclusion data

The Laminaria and Corallina oil fields represent classic fault-bounded closures (horst blocks) that contain the highly productive Callovian reservoir sands. Their complicated charge and retention history with evidence of larger paleoaccumulations below the present-day oil column is typical of the northern Bonaparte Basin.

The charge history of the Laminaria and Corallina fields has been constrained by an integration of fluid-inclusion data with conventional oil shows and wireline log data. The distribution of the current and paleohydrocarbon accumulations is used to calibrate the outcome of the coupled geomechanical model. Fluid-inclusion results from additional exploration wells over the Laminaria High and Nancar Trough (de Ruig et al., 2000; Gartrell et al., 2006) are also summarized to augment the distribution of breached structures. All depths given are in true vertical depth measured from a datum of mean sea level (TVDSS).

GOI results from the Laminaria oil field

GOI results across three wells and from 31 samples are integrated to constrain the oil-charge history of the Laminaria field (Figure 5). The Laminaria-2 well is located in the eastern part of the Laminaria field (Figure 2). The top of the reservoir is at 3177 m (10,421 ft), and the current free-water level (FWL) is at 3286 m (10,778 ft). High GOI values between 7.0% and 20.2%, consistent with high oil saturation and a paleo-oil column, are recorded down to 3297 m (10,814 ft). An anomalous sample (GOI value = 0.1%) at 3254 m (10,673 ft) correlates with a lower-quality reservoir and may represent a small zone of lowered paleo-oil saturation within an otherwise continuous zone of high paleo-oil saturation. The sharp drop to low GOI values recorded in all samples from below 3308 m (10,850 ft) (0.0%–0.1%) is interpreted to represent the crossing of a paleo-OWC, defining an 11–22-m (36–72-ft) residual oil column. The intermediate GOI value (2.2%) recorded in the uppermost sample corresponds to a shale-prone section, and the smaller GOI value probably reflects reduced reservoir properties that would have resulted in lower oil saturation.

The Laminaria-4 well is located in the northern part of the Laminaria field (Figure 2). The top of the reservoir is at 3278 m (10,752 ft), and the current FWL is at 3282 m (10,765 ft). High GOI values between 9.0% and 56.4%, consistent with high oil saturation and a paleo-oil column, are recorded down to 3294 m (10,804 ft). The drop in GOI values below this point (<0.1% and 1.3%) is interpreted to represent the crossing of a paleo-OWC and constraint to a 9–12-m (30–39-ft) residual oil column. Samples near the top of the reservoir show a low-to-intermediate GOI value (<0.1% and 2.2%), consistent with low paleo-oil saturation. Measured permeability (5 and 87 md) is much lower than the typical reservoir value (>500 md; Woodside Offshore Petroleum Pty. Ltd., personal communication, 1997); as such, this zone may be associated with high capillary entry pressures, which reduced paleo-oil saturation.

The Laminaria East-1 well is located in the eastern part of the Laminaria field. The top of the reservoir is at 3262 m (10,699 ft), and the current FWL is at 3295 m (10,808 ft). Two core samples between 3280 and 3286 m (10,758 and 10,780 ft) have GOI values of 9.2% and 6.2%, consistent with high oil saturation and the presence of paleo-oil down to at least 3286 m (10,780 ft). Low GOI values were not obtained below this depth, so the position of the paleo-OWC is not constrained in this well. Two core samples taken near the top of the reservoir have GOI values of 0.5% and 0.1%, respectively, which is consistent with a zone of low oil saturation. Both of these samples have significantly lower permeability (0.1 and 51 md) than the samples below (572 and 900 md); therefore, the low GOI values equate with a zone of reduced oil saturation due to poor reservoir quality. The slight variation in FWL across the Laminaria field is related to the hydraulic head distribution in the underlying aquifer (Underschultz, 2005).

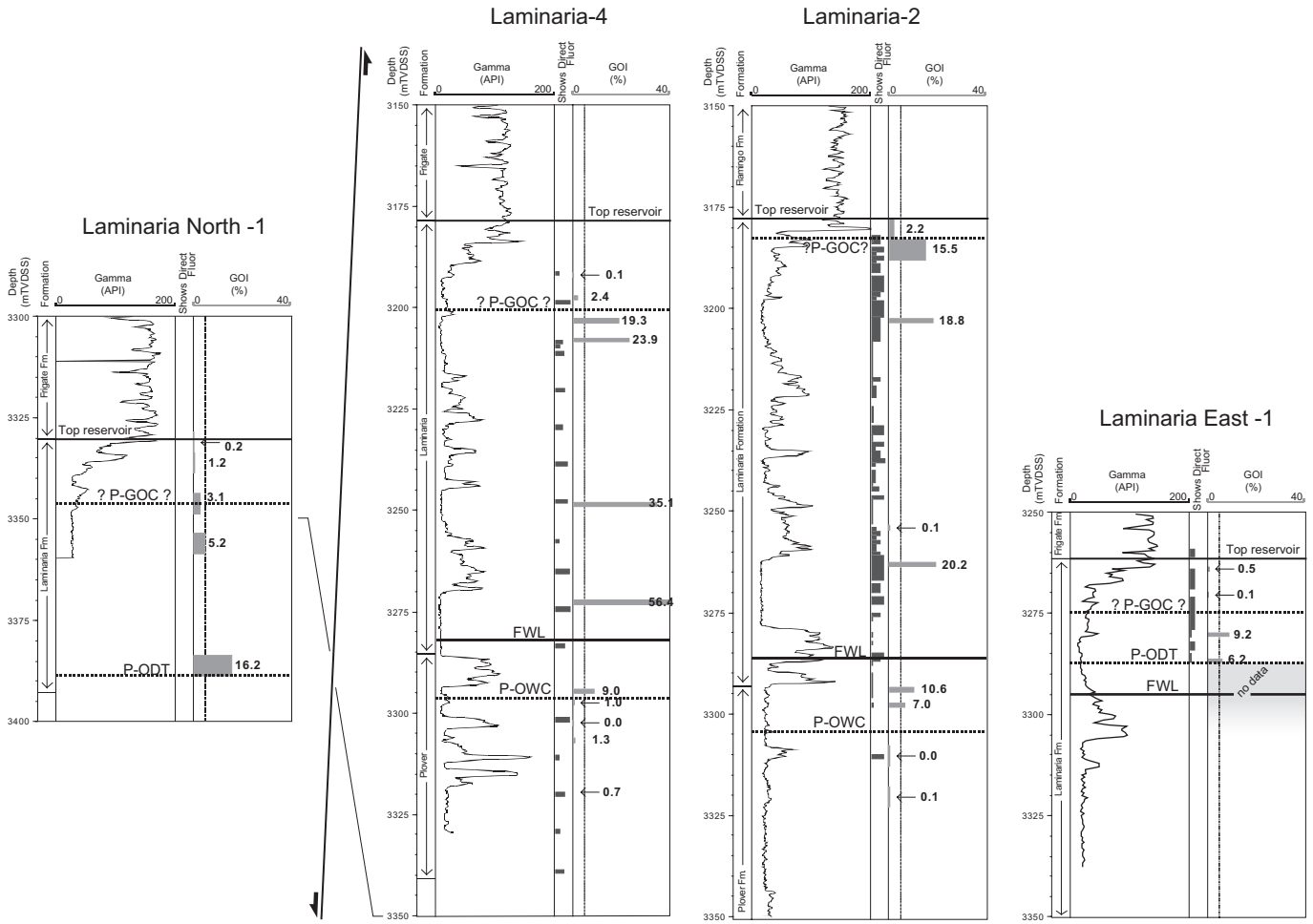

Figure 5. Laminaria field and Laminaria North structure, sample location, and GOI results for Laminaria-2, Laminaria-4, Laminaria East-1, and Laminaria North-1. P-GOC = paleo-gas/oil contact, P-OWC = paleo-oil/water contact, P-ODT = paleo-oil down to, FWL = free water level. See Figure 2 for well locations.

The Laminaria North-1 well is located north of the Laminaria field on the adjacent fault block (Figure 2). The reservoir section is currently dry. Cuttings samples between 3353 and 3358 m (10,998 and 11,014 ft) and between 3383 and 3388 m (11,096 and 11,113 ft) have GOI values of 5.2% and 16.2%, respectively, consistent with high oil saturation and the presence of a paleo-oil column that extends down to the total depth (TD) of the well. This suggests the loss of at least 30 m (98 ft) of hydrocarbon column.

GOI results from the Corallina oil field

GOI results taken from two wells and involving 20 samples have been integrated to constrain the oil-charge history of the Corallina field (Figure 6).

The Corallina-1 well is located in the central part of the Corallina field (Figure 2) and contains an oil column with an FWL at 3210 m (10,529 ft). Five new samples have been taken to better constrain the position of the paleo-hydrocarbon contacts previously defined by Dutkiewicz and Eadington (1997). High GOI values above the 5% threshold and consistent with the attainment of high oil saturation and a paleo-oil column are defined between the top of the reservoir at 3140 m (10,299 ft) and 3260 m (10,693 ft). Two of the samples from this interval contain lower GOI values (0.1% and 3%) and indicate zones of reduced paleo-oil saturation within the paleo-oil column. The drop in GOI values below 3260 m (10,693 ft) is interpreted to represent the crossing of a paleo-OWC, and a 50–55-m (164–180-ft) residual oil column is inferred. Deeper samples at 3265 m (10,709 ft) have low GOI values between 0.2% and 0.5% and are consistent with low oil saturation and a paleowater zone.

The Corallina-2 well is located in the northern part of the Corallina field (Figure 2) and contains an oil column with an FWL at 3210 m (10,529 ft). Samples from the top of

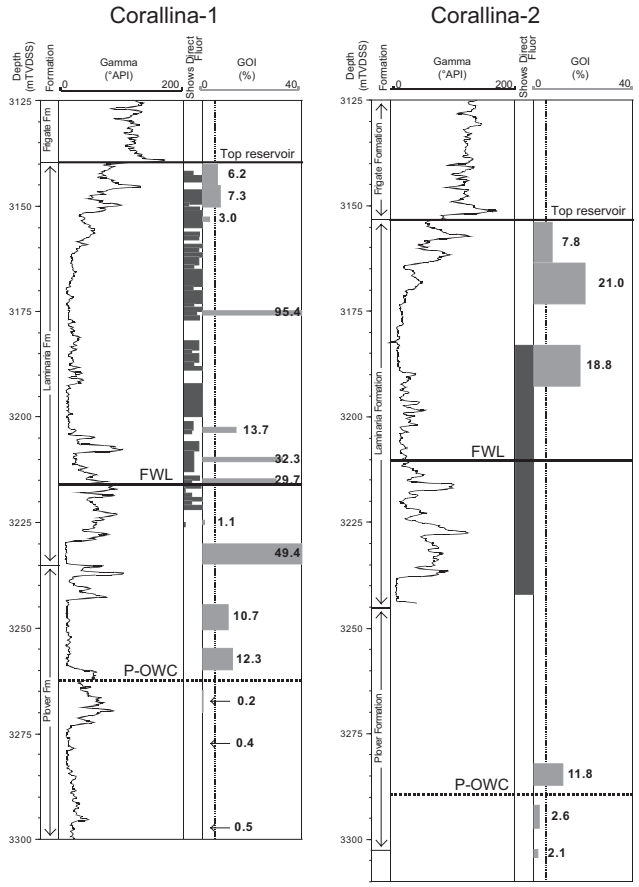

Figure 6. Corallina field, sample location, and GOI results. P-OWC = paleo-oil/water contact, FWL = free water level. See Figure 2 for well locations.

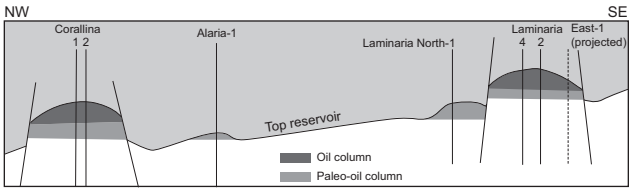

Figure 7. Schematic cross section across the Laminaria High and distribution to present-day and P-OWC contacts.

Table 1. Laminaria High and Nancar Trough exploration well results.

Prospect	Charge
Alaria	Dry with paleo-oil column, breached or off structure
Bogong	Dry with paleo-oil column, breached
Buang	Dry with paleo-oil column, breached
Buffalo	50-m (164-ft) oil column with paleo-oil column
Buller	27-m (89-ft) oil column with paleo-oil column
Capung	Dry with oil shows, breached
Claudea	Dry with no hydrocarbon shows, lack of charge
Jahal	30-m (100-ft) oil column with paleo-oil column
Vidalia	Dry with small paleo-oil column (gas/oil interface), breached

the reservoir down to 3287 m (10,781 ft) have high GOI values (7.8%–21%), consistent with high oil saturation and the presence of a paleo-oil column. The drop in GOI values below 3287 m (10,781 ft) is interpreted to represent the crossing of a paleo-OWC and the presence of a paleowater zone. The paleo-OWC represents a 72–82-m (236–269-ft) residual oil column.

Charge reconstruction summary

The GOI data for the Laminaria and Corallina fields are consistent with the presence of a paleo-oil column below the current OWCs. Across the Laminaria field, GOI results from Laminaria-2 and -4 suggest a 9–22-m (30–72-ft) paleo-oil column in the Laminaria field below the present-day FWL. The GOI data also indicate that the block to the north of the Laminaria field was initially charged, with the currently dry Laminaria North-1 well containing a paleo-oil column. In the Corallina field, the GOI data define a paleo-oil column below the current approximately 77-m (~253-ft) oil column (de Ruig et al., 2000) of between about 50 and 82 m (164 and 269 ft).

The low GOI values recorded at the top of the reservoir in the Laminaria field and in Laminaria North-1 most likely reflect the effect of poor reservoir quality, causing lowered oil saturation. Alternatively, the values could imply that a small paleogas cap overlies the paleo-oil zones. Similar low GOI values are recorded in the uppermost samples from the Alaria-1 paleo-oil zone located northwest of the Laminaria field and southwest of the Corallina field.

These observations, together with other GOI results from wells across the northern Bonaparte Basin (i.e., Brincat et al., 2001), suggest that the original oil charge was more extensive than is represented by the current oil columns and that fields such as the Laminaria and Corallina initially were filled to a deeper level than presently recorded by the reservoir crude oil (Figure 7; George et al., 2004). Additional fluid-inclusion data from the Laminaria High and the Nancar Trough (Table 1) show evidence for paleo-oil columns below present accumulations in other oil fields (Buffalo, Jahal) and paleo-oil columns in several dry structures (e.g., Brincat et al., 2004; Gartrell et al., 2006).

The paleo-OWCs in the west of the Corallina and Laminaria fields (Corallina-1 and Laminaria-4 wells) are shallower than the easterly wells (Corallina-2 and Laminaria-2). This variation may indicate some degree of general easterly tilt after the original charge, as observed on the Griffin field in the northern Carnarvon Basin (Brincat et al., 2006). However, postcharge tilting does not appear to represent a major contributor to oil loss because the structures are not currently filled to spill. For tilting and lateral remigration to be the sole reason for oil loss, then, we would expect that the fields would be at spill point today.

Coupled numerical modeling

We constructed a coupled deformation and fluid-flow model for the Laminaria and Corallina fields to assess postreactivation strain distribution and to address the impact on the retention of hydrocarbons.

Model architecture and properties

To build a coherent 3D mesh, some simplifications of the stratigraphic and structural architecture were required. The 3D model for the $50 \times 25 \times 10$-km ($31 \times 15.5 \times 6.2$-mile) Laminaria-Corallina area contains nine main faults (Figure 8), mapped as continuous fault surfaces; several subsidiary faults were ignored. Although the base of all of the faults is located at the 5-km (3.1-mile) depth level throughout the model, the upper fault-tip elevations are variable, as determined from the shallowest part of each fault from the seismic interpretation (Figure 4). The fault dip varies from 45° to 65° in accordance with depth-converted structural interpretation. The top-reservoir and top-seal horizons were filtered to remove local sharp geometric spikes.

The stratigraphic framework of the model has been simplified to reflect the broad configuration of mechanical layers in the area. This framework consists of four rock units (Table 2): (1) a top carbonate layer, (2) a middle shale layer acting as the regional seal, (3) a sandstone unit including the reservoir, and (4) a relatively weak basal rock unit incorporated to reduce the edge effects when faults reach the model base. The thicknesses of these units are variable and are defined from the seismic data interpretation (Figure 3).

Each rock unit is assigned with specific mechanical and fluid-flow properties (Table 2), based on data from literature or rock-property data for the region (CSIRO unpublished data, 2007).

Faults are represented by narrow zones with predeformation permeability identical to the host rocks (Table 2) and with low strength. In this study, we adopt a simple approach to allow fault permeability to change with shear strain (see "Fault-Permeability Variation Scheme" below for details). During the deformation of the model, dilation and shearing deformation develop as a result of incorporating small positive dilation angles (Table 2) that are kept

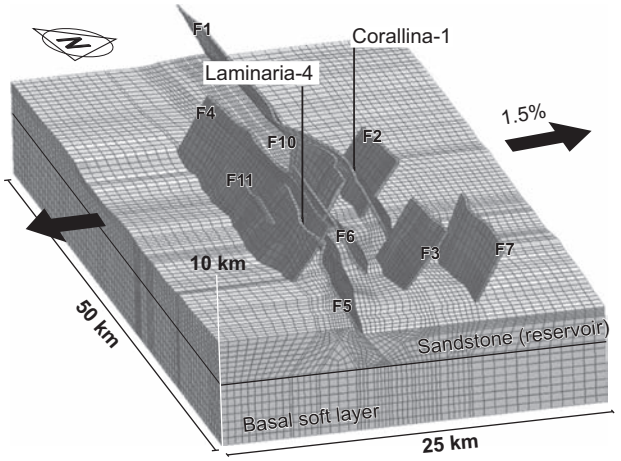

Figure 8. Geometry of the 3D numerical model. The upper shale and carbonate layers are omitted to illustrate fault geometries. The extension direction is given by the thick black arrows arrows. Fault numbers are also shown.

Table 2. Initial material properties of the 3D Laminaria High numerical model.

Model unit	Density (kg/m^3)	Young's modulus (GPa)	Poisson's ratio	Cohesion (MPa)	Tensile strength (MPa)	Permeability (m^2)	Porosity (%)	Friction angle (°)	Dilation angle (°)
Carbonate	2500	40	0.20	17.50	8.75	5×10^{-15}	0.30	30	2
Shale	2400	2	0.35	2.75	1.38	1×10^{-19}	0.15	22	2
Sandstone	2450	25	0.25	15.00	7.50	1×10^{-14}	0.18	30	2
Basal unit	2550	2	0.20	2.00	1.00	1×10^{-19}	0.05	20	0
Faults	2300	1	0.15	1.00	0.50	Various	0.20	15	3

constant throughout simulation. We consider this assumption reasonable because of the small regional deformation of the model (1.5% bulk extension).

Boundary conditions

The Tertiary reactivation in the Timor Sea was dominated by an extensional stress regime with approximately normal reactivation of rift faults (Gartrell and Lisk, 2005; Gartrell et al., 2006). We simulate an approximation of this regime in the model by applying constant extensional displacement rates normal to the north and south edges. The maximum bulk extensional strain for the model aimed to achieve is approximately 1.5%.

The initial condition for formation-water pore pressure in the model is derived from local in situ pressure data from the Laminaria High area (Figure 9). A hydrostatic fluid-pressure gradient (0.433 psi/ft or 9.81 kPa/m) is set between the seafloor and the top seal (top of the shale layer). Based on a characteristic hydraulic head of approximately 70 m (239 ft) for the top of the Laminaria Formation or the base of the shale for the study area, a vertical pressure gradient within the shale of 0.466 psi/ft or 10.57 kPa/m is defined. For the sandstone layer, we use a slightly overpressured gradient (0.439 psi/ft or 9.95 kPa/m). These initial pore-pressure conditions define a vertical hydraulic-head gradient across the shale that results in upward vertical flow.

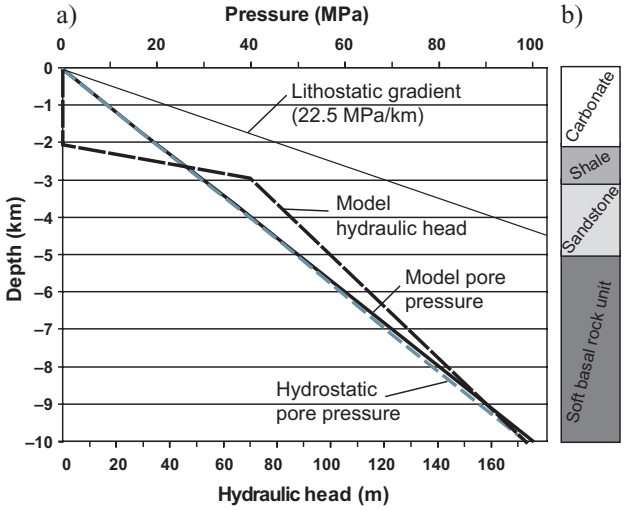

Figure 9. Initial pressure condition for the numerical model. (a) Pore-pressure gradient (heavy solid black line) and hydraulic head (broken black line) used in the numerical model; the hydrostatic pore pressure (broken gray line) and lithostatic gradient (thin solid line) are also plotted for reference. The model gradient represents a slightly overpressured system in the rocks below the carbonate unit. (b) Stratigraphic units used in the numerical model.

Additional boundary conditions include a free-surface condition for the model top, a fixed-model base in the vertical direction (but free movement in the horizontal direction), and fixed-model east and west edges in the east–west direction (free movement in the north–south extensional direction). These boundary conditions are similar to those used by Zhang et al. (2009).

Postreactivation throw and strains

All faults included in the model were activated and accumulated new displacement during the deformation. This outcome is consistent with regional seismic interpretations that all faults are reactivated to some degree (Gartrell and Lisk, 2005; Gartrell et al., 2006). The postdeformation throw distribution from the model is also regionally consistent with the displacement profiles observed on seismic data (Figure 10). This consistency suggests that the modeling run is able to reasonably simulate deformation distribution and strain portioning among the major faults across the study area. Shear and volumetric strains are computed and plotted after 1.5% bulk extension (Figure 11). Their gross distributions are similar, with higher dilatational and contractional volumetric strains associated with fault segments that exhibit the greatest shear strains. The volumetric strain distribution at the top reservoir level shows dilation (values > 0) in the fault zones coupled with areas of contraction (values < 0) in the hanging-wall blocks (Figure 11c). These patterns suggest that fault zones are predominantly dilatational during extensional reactivation, but contractional zones can develop within the hanging-wall blocks of faults as a result of normal fault movement and rotation.

Shear strain is primarily localized on larger faults, but the lateral distribution is clearly heterogeneous along individual fault planes (Figure 11b). The large faults (F1, F4, and F5 in Figure 11) delimiting the Laminaria and Corallina oil fields accommodated most of the postrift extensional reactivation and associated shear strain. More importantly, they also exhibit sharp and significant shear-strain variations along strike, especially where fault tips overlap. This process creates shielded areas, with low shear-strain values that correlate with the location of the two oil fields (Figure 11a and 11b).

The Laminaria field is delimited to the north by the north-dipping fault F5 that exhibits a rapid drop of shear strain values at its western tip where it overlaps with faults F4 and F6 (Figure 11a). To the south, the present-day field is delimited by a splay branch connected with F4 that was not initially incorporated into the numerical model. How-

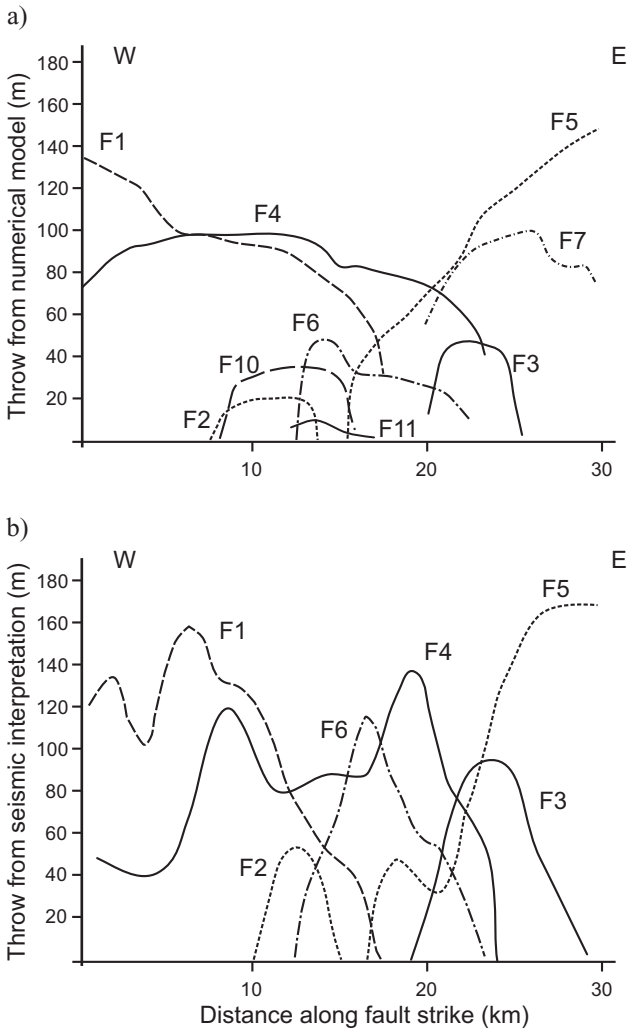

Figure 10. Plots of fault throw at the top of the reservoir (vertical components of displacement along faults) versus distance (along fault-strike length). (a) Throw output of the deformation numerical modeling. (b) Throw interpreted from 3D seismic over the Laminaria High.

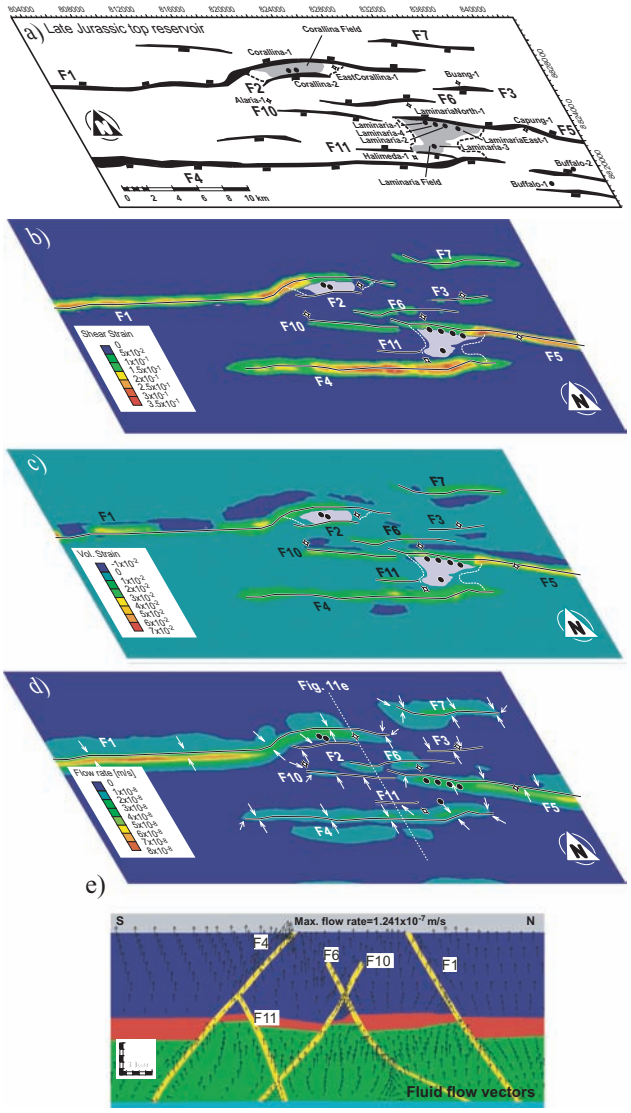

Figure 11. Correlation of oilfield architecture and numerical model results after 1.5% bulk extension. (a) Structural framework at the Late Jurassic top-of-reservoir level. (b) Shear-strain distribution at the top sandstone level (reservoir) in plan view. (c) Volumetric strain patterns at the top-of-sandstone level (reservoir) in plan view. (d) Fluid-flow-rate distribution and schematic flow vectors (white arrows) in plan view. (e) Fluid-flow-velocity distribution on a south–north cross section. Located on Figure 11d.

ever, the splay is regarded as a low-strain structure because of the extensive deformation accommodated by the F4 splay as well as the behavior of the neighboring fault F11 that has roughly similar size and geometry as the splay and displays low shear and volumetric strains.

The eastern part of fault F1 also exhibits a sharp drop of shear strain where it overlaps with the central part of faults F2 and F10 (Figure 11a and 11b). This drop correlates with the location of the present-day Corallina field. A locus of high shear-strain values is located on F1 directly west of the Corallina field; it develops over a jog forming a connection zone between two rift-fault segments. A similar process is also visible on F4 and F7, where relatively high shear-strain values correlate with fault corrugations.

Fault-permeability variation scheme

Prior to deformation in the model, the continuous fault zones have permeabilities identical to those of their host rocks, allowing cross-fault migration at points of juxtaposition but preventing upfault leakage across the top seal.

Based on findings from generic models (Zhang et al., 2009), leakage mechanisms inferred from regional studies

(Smith et al., 1996; de Ruig et al., 2000; Gartrell et al., 2006, Ciftci and Langhi, 2012) and based on the observed correlations between computed shear strain and preserved hydrocarbon accumulations on the Laminaria High (see "Postreactivation Throw and Strain" and "Discussion"), we have incorporated a fault-permeability variation scheme for the fluid-flow modeling in which fault permeability increases with accumulation of shear strain (approximately reflecting shear-induced dilation and permeability enhancement). Following reactivation, the maximum fault permeability with shear strain or shear failure in respective host rocks is 2.0×10^{-14} m^2 (2.15×10^{-12} ft^2 or 2.03×10^{-2}d) in carbonate; 1.0×10^{-15} m^2 (1.07×10^{-13} ft^2 or 1.01×10^{-3}d) in shale; and no change in sandstone and soft basal unit (still 1.0×10^{-14} m^2 [1.07×10^{-12} ft^2 or 1.01×10^{-2}d] and 1.0×10^{-19} m^2 [1.07×10^{-17} ft^2 or 1.01×10^{-7}d], respectively; permeability is in m^2 with the relationship 1 d = 9.8697×10^{-13} m^2 [1 d = 1.0624×10^{-10} ft^2]). This simplistic relationship captures the increase of structural permeability with initial shearing accumulation along faults, in turn leading to the improved connectivity of the fault/fracture networks through the top seal (de Ruig et al., 2000; Gartrell et al., 2006; Ciftci and Langhi, 2010, 2012).

The approximation is reasonable for a model with relatively small bulk extension (i.e., corresponding to an early phase of fault reactivation). It is consistent with the general expectation that low-permeability rocks would initially experience permeability increase when involved in shearing deformation (e.g., shearing fractured shale) and is also consistent with the experimental results of Zhang and Cox (2000), showing permeability enhancement in a synthetic mud with shearing deformation. Permeability reduction in fault zones is possible at a later faulting or high shearing stage with the development of fine-grained fault gouge.

Fluid-flow pattern

Following the fault-permeability variation scheme, the modeled fluid flux within the reservoir after 1.5% extension is greatest in the vicinity of high-strain fault segments (Figure 11d). Flow vectors usually are directed perpendicularly toward fault strike from footwall and hanging-wall blocks. At the proximity of a fault's end, lateral fluid convergence toward fault tips is usually observed. As reported from generic numerical models with simple fault geometries and similar gross mechanical stratigraphy to the present model (Zhang et al., 2009), higher regional vertical fluid flux is associated with larger faults as a result of greater shear and dilatational strain and permeability enhancement. However, fluid flux along faults is inhomogeneous, with greater flux through fault segments accommodating more shear and volumetric strains. Upward flow is modeled within faults and host rocks (Figure 11e) due to the pore-pressure gradient used as a boundary condition, with slightly higher pore-pressure gradient in the reservoir rocks below the shale section. However, upward fluid migration through the shale is predominantly through faults — in particular, the large faults. Fluid flow in the sandstone unit (reservoir rocks) shows a clear pattern of convergence toward the faults.

Seismic expression of leakage and discharge sites

Fluid remigration from the Jurassic reservoir is investigated over the Laminaria and Corallina fields to calibrate the coupled geomechanical model and the relationship linking reactivation shear strain and enhanced structural permeability.

Blind discharge sites (buried thief zones), expulsion sites at paleo- or (near) the present-day seafloor, and hydrocarbon chimneys are inferred from seismic interpretations and are constrained with lithology reported from wells and regional structural history. The recognition of these seismic facies, assessment of their 3D distribution, and spatial relationship to the structural elements are calibrated against the charge history from the fluid-inclusion data and the existing trap integrity models to better constrain and predict the regional remigration system.

Distribution of leakage indicators

Three distinct stratigraphic levels (near seabed, base of the Barracouta Formation, and the Oliver Sandstone; see Figures 3 and 4) display seismic anomalies that are spatially associated with the structural network, suggesting a relationship between upfault fluid migration and discharge into buried thief zones or through loss at the free surface (Figure 4). In addition, two further levels (i.e., Late Miocene unconformity and Grebe Sandstone) present sporadic seismic anomalies (Figure 4); however, these are considered minor and are not discussed here.

Interpreted near-present-day seabed expulsion sites

Seismic bright spots at the seabed have long been recognized in the North Sea and the Gulf of Mexico, where they are related to petroleum remigration and seepage promoting production of authigenic carbonate (Hovland

et al., 1985; Dando et al., 1991; Roberts et al., 2006). Similar facies have been reported from the Yampi Shelf (about 300 km south-southwest of the Laminaria High; Figure 1) and are also inferred to be associated with expulsion of hydrocarbons (Cowley and O'Brien, 2000; Rollet et al., 2006). In the subject area, this relationship is further strengthened by the observation of free gas plumes seen in the water column on echo sounder data (Rollet et al., 2006). Reflectivity extractions derived from spectral decomposition amplitude horizon slices (Partyka et al., 1999; Giroldi et al., 2005) over the Laminaria and Corallina fields show that the reflectivity distribution of the near-seabed reflectors is clearly heterogeneous and is tightly controlled by the structural network (Langhi, 2009; Figure 12). We interpret these bright spots to be indications of hydrocarbon remigration from the reservoir, based on the distribution and the similarity with previously reported seafloor bright spots (Hovland et al., 1985; Dando et al., 1991; Roberts et al., 2006).

The downdip side of the present-day Laminaria field is bounded by a fault splay branch that connects laterally with fault F4 (Figure 2). Based on the paleo-OWC definition from the fluid inclusion data, the Laminaria paleofield extended farther to the east and was likely initially delimited by F4. Vertically, F4 is connected with a series of right-stepping en echelon faults that propagate through the Cenozoic up to the sediment-water interface, where it corresponds to the location of seafloor bright spots in the vicinity of the Laminaria field (Figure 12). In addition to recording paleoleakage, this observation could indicate present-day fluid leakage associated with the high reactivation shear strain currently acting on fault F4 (Figures 4, 11, and 12).

The seafloor reflectivity along F5, bounding the crestal side of the Laminaria field, is more difficult to ascertain because of the presence of a large carbonate shoal that obscures and degrades the seismic signal below (Figure 12). However, the western en echelon Cenozoic segments of F5 appear to display slightly less reflectivity compared to the background (Figure 12). This decrease in reflectivity could indicate more restricted fluid migration at the western end of the fault plane, where reactivation shear strain drops off. A carbonate shoal is delimited by the eastern part of F5 that connects downdip with the Jurassic segment bounding the underlying dry Capung structure; the segment has high reactivation shear-strain values and from fluid-inclusion data shows evidence of a paleo-oil column.

Seafloor bright spots west and east of the Corallina field along fault F1 (the north-bounding fault of the field; Figure 12) suggest a lateral variation of structural permeability along the structure that correlates with a decrease of strain distribution where F1 overlaps with F2 and F10. A moderate reflectivity anomaly is present along the Cenozoic segments of F3 that delimits the dry but previously charged (Dutkiewicz et al., 1997) Buang structure (Figure 12). This anomaly correlates with a local increase in modeled reactivation shear strain (Figure 11).

Seafloor bright spots are also associated with the Vidalia structure (Figure 12). However, unlike the pattern observed above the Corallina discovery, the reflectivity does not grow dim above the closure but increases in intensity, forming a strong anomaly that follows the trend of the main bounding faults. This anomaly suggests extensive upfault remigration from the Vidalia closure (dry with probable indication of paleo-oil column; Brincat and Eadington, 1998).

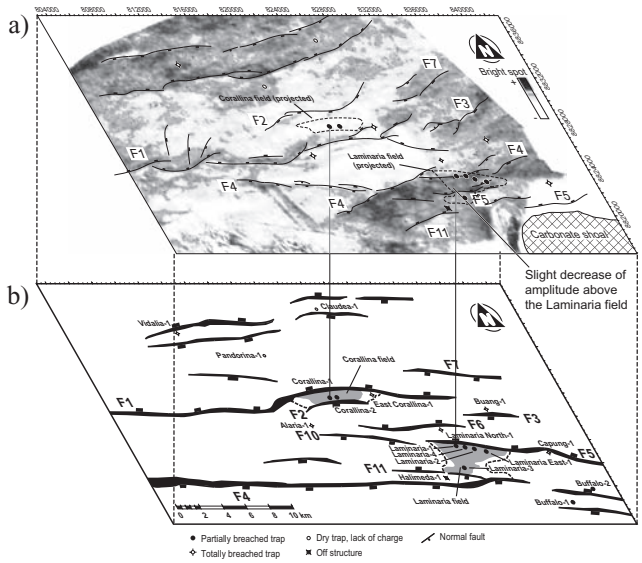

Figure 12. Reflectivity at seabed above the Laminaria and Corallina fields. (a) Extraction from spectral decomposition amplitude horizon slices at 30 Hz for the seabed. (b) Structural framework at the Late Jurassic reservoir level. The seabed bright spots are controlled by the structural network and interpreted as indications of hydrocarbon remigration from the reservoir.

Interpreted Miocene-Pliocene expulsion sites

Seismic anomalies that locally recorded the main pulse of deformation due to fault reactivation are present at the Miocene-Pliocene interface (base of Barracouta Formation; see Figures 3 and 4) (Langhi et al., 2011). These anomalies constitute seismic facies with high reflectivity and high signal coherency and are interpreted as authigenic

carbonate hardgrounds and/or buildups aligned along conductive fault planes. It has been proposed (Hovland et al., 1994; O'Brien et al., 2002; Bailey et al., 2003; Rollet et al., 2006) that coral reef growth might be linked with escaped hydrocarbon or gas hydrates acting as a nutrient source. The Miocene-Pliocene anomalies have been recognized mostly over the Laminaria High (Figure 13), although the development of modern carbonate shoals in the vicinity of the present-day shelf edge creates velocity artifacts in the subsurface. Stratigraphic features (e.g., channels, fans) that impact the coherence of the seismic data can also obscure or disrupt the seepage pattern locally (Figure 13).

Localized anomalies are associated with the eastern part of fault F4 that bounded the downdip side of the Laminaria paleofield, and the anomalies experience high shear strain in the model (Figure 11; ① in Figure 13). No significant anomaly is associated with the western end of F5, supporting the assumption that this fault segment has not leaked due to lower shear-strain accommodation (Figure 13). West of the Laminaria field, an anomaly is located along the Cenozoic segment of fault F4 (② in Figure 13) and again correlates with high shear strain in the model (Figure 11).

Widespread scattered amplitude anomalies are present over the Corallina field (③ in Figure 13) and expand east and west, following the trend of the reservoir-bounding faults (F1 and F2; Figure 13). The detailed 3D morphology, internal pattern, and seismic signature suggest that this facies represents constructed carbonate platforms (Figures 14 and 15) that develop in response to the first hydrocarbon seepage at the time of initial fault reactivation. At the Miocene-Pliocene interface, anomalies are present along the western part of F1, following the pattern observed on the seafloor and suggesting local enhancement of structural permeability (④ in Figure 13). However, seismic facies with high reflectivity and coherency are also distributed at the location of the present-day field (③ in Figure 13), suggesting at least some episodic fluid migration at that location. Fluid migration along the low reactivation shear-strain fault F2 cannot be precluded based on the Miocene-Pliocene anomalies' distribution.

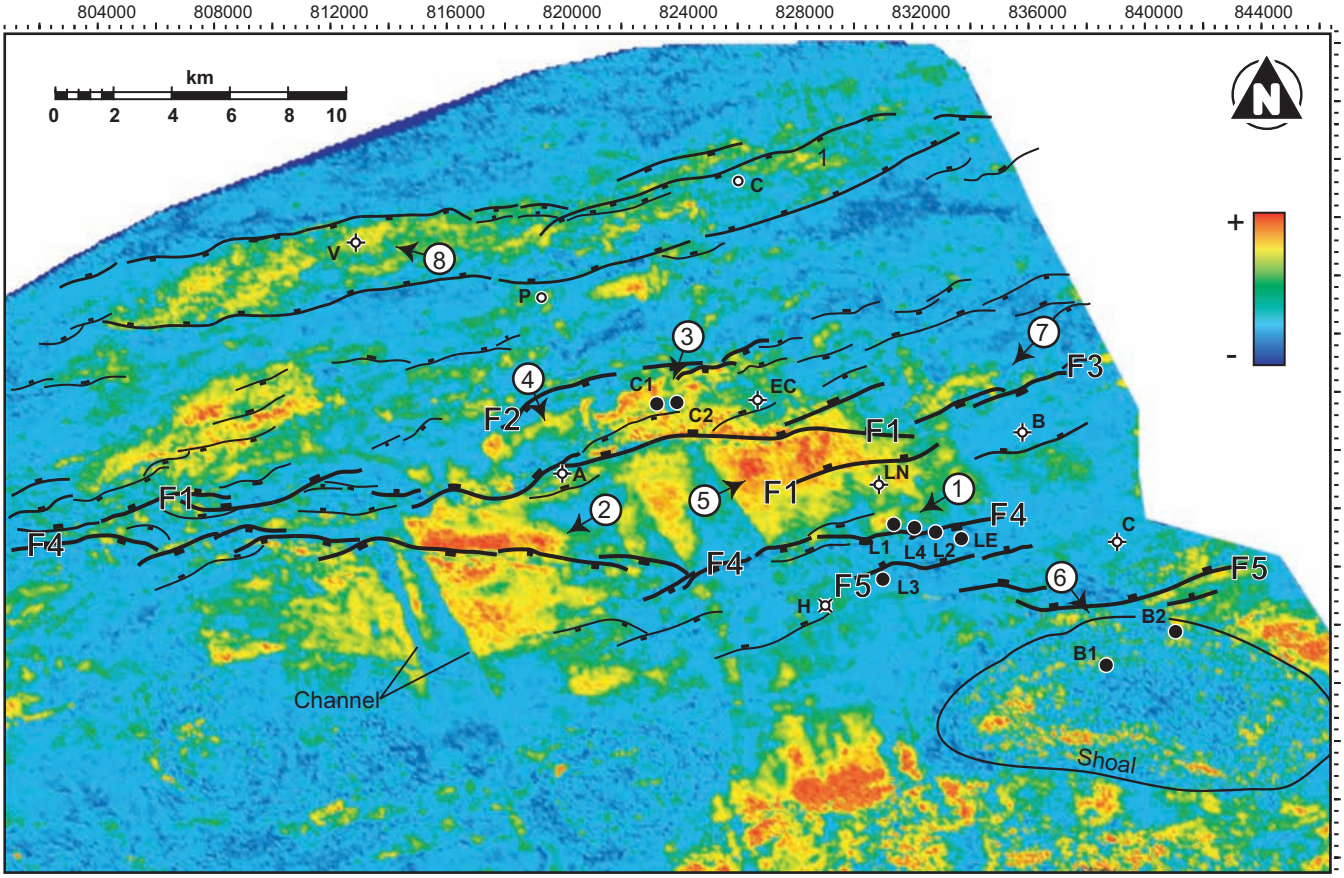

Figure 13. Average reflection strength over a 30-ms window 20 ms above the Miocene-Pliocene boundary, showing amplitude anomalies interpreted as authigenic carbonate hardgrounds and/or buildups aligned along conductive fault planes. See text for reference to numbers ①–⑧.

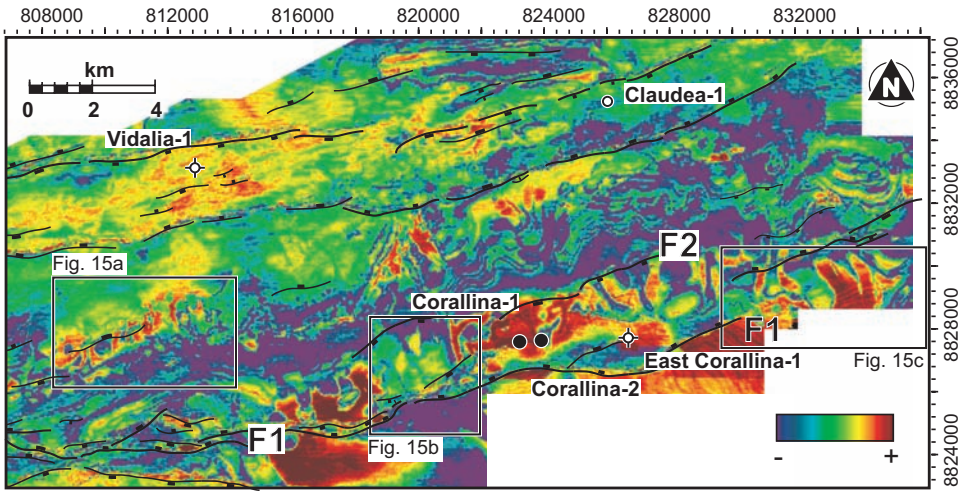

Figure 14. Detailed reflection strength map extracted 20 ms above the Miocene-Pliocene boundary in the vicinity of the Corallina field, showing the detailed morphology of amplitude anomalies interpreted as constructed carbonate platforms developing in response to hydrocarbon seepage at the time of initial fault reactivation.

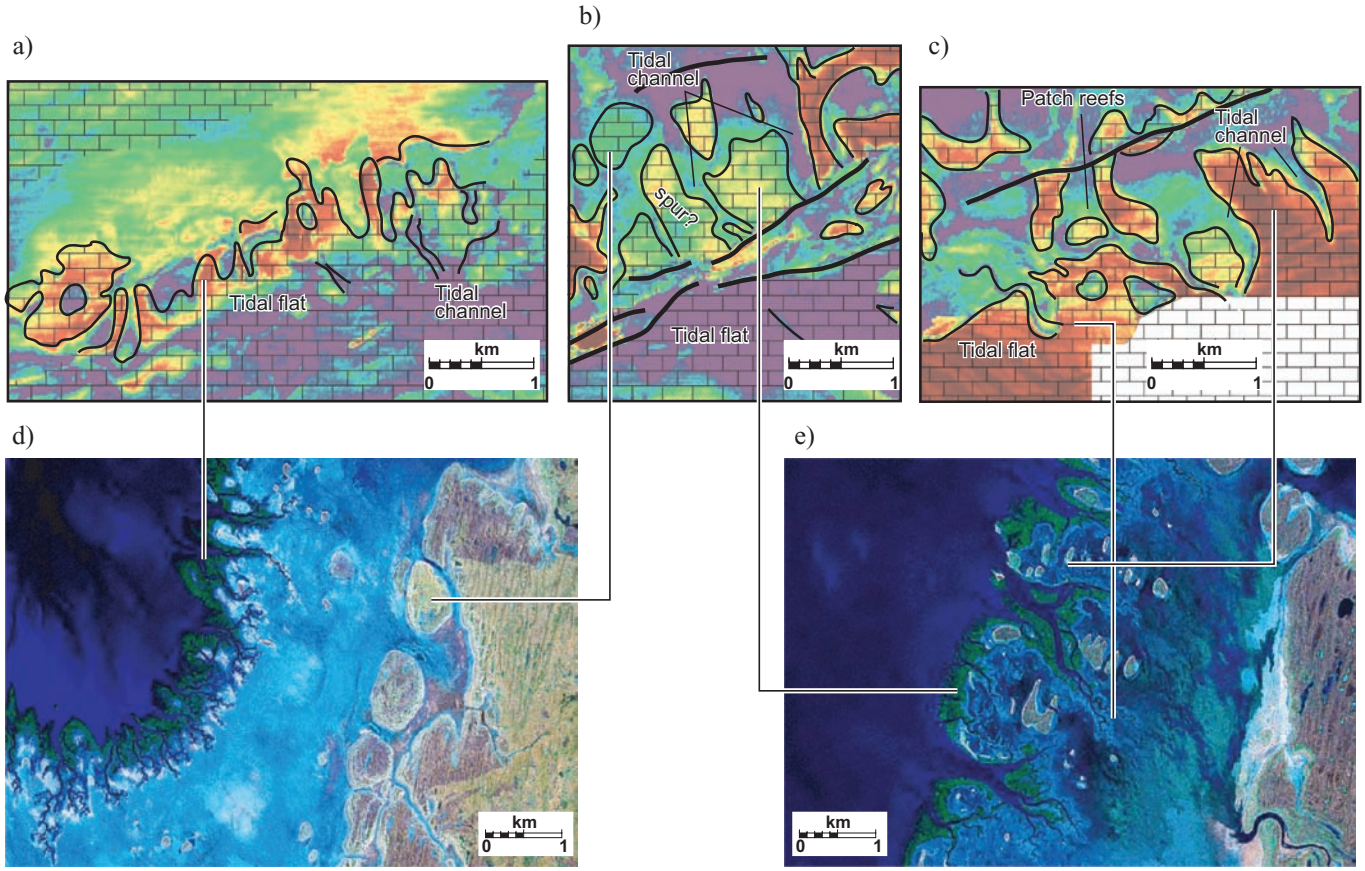

Figure 15. Comparison between Miocene-Pliocene morphology and present-day example of a constructed carbonate platform. (a-c) Details of the reflection strength map, located on Figure 14. (e-f) Satellite images of the coastline in the Exmouth Gulf, Western Australia.

A large anomaly is located to the east of the Corallina field and north of the Laminaria field (⑤ in Figure 13). It is well delimited to the north by the main fault segment forming the eastern end of F1 (low modeled shear-strain fault segment east of the Corallina field, Figure 11). To the south, the anomaly is bounded by another Cenozoic overlapping fault segment, forming a local relay zone (Figure 13). The base of the Barracouta Formation seismic signature for the completely breached Buang and Capung traps varies from a diffuse anomaly feeding the overlying shoal near Capung-1

(⑥ in Figure 13) and a restricted local reflectivity anomaly above Buang-1 (⑦ in Figure 13).

Over the Vidalia-Claudea trend, the seismic signature evolves with the high-energy and coherent facies, well developed over the Vidalia structure (⑧ in Figure 13) but growing dim over the Claudea structure. This variation might not relate to lateral variation of fault permeability but rather to the lack of charge, as highlighted by fluid inclusion data (Vidalia-1 records a small paleo-oil column, but Claudea-1 does not).

Oliver basal member discharge site

In the Timor Sea, rising sea level during the Early Miocene inundated the shelf but was punctuated by intervening periods of lowstand that allowed the deposition of the Oliver basal sandstone member overlying the Eocene carbonates (Pattillo and Nicholls, 1990; see Figures 3 and 4). The distribution of this sandstone can be locally restricted due to sediment bypass and reduction of sediment supply. On the Laminaria High, the sandstone member is only found south and east of the Laminaria field; the wells to the north and east commonly show a friable calcarenite, equivalent to the sandstone member at the base of the Oliver Formation. Stronger and broader reflections typically controlled by the structural network are present within the Oliver basal member and are interpreted as indications of upfault fluid migration and charging of this porous formation laterally (Figure 16). Amplitude and sweetness (instantaneous amplitude divided by the square root of the instantaneous frequency) are used to assess the distribution of these anomalies.

A series of strong anomalies, located east of the Laminaria field, correlates with the part of fault F4 that delimited the Laminaria paleofield (① in Figures 16 and 17). These anomalies, associated with a local increase in reactivational shear strain (Figure 11) on that fault segment (Figure 17b), suggest a local improvement of structural permeability and discharge of hydrocarbon within the sandstone forming the Oliver basal member east of the Laminaria field (e.g., Laminaria East-1; BHP, 1996). This anomaly continues to the east, where it is related to

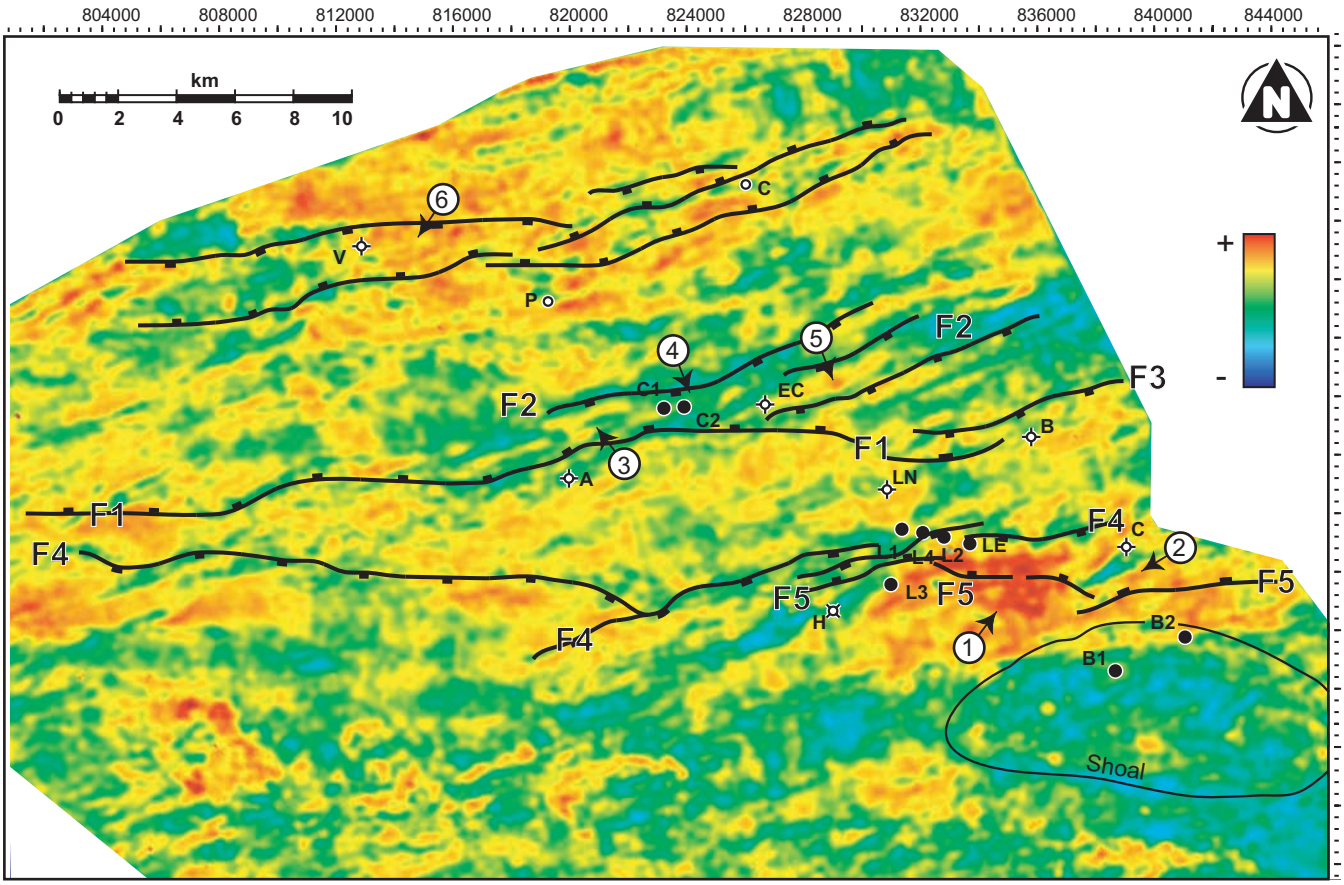

Figure 16. Sweetness map in the Oliver basal member over the study area. The bright spots might indicate fluids migrating upfault and charging the porous formation laterally. See text for reference to numbers ①–⑥.

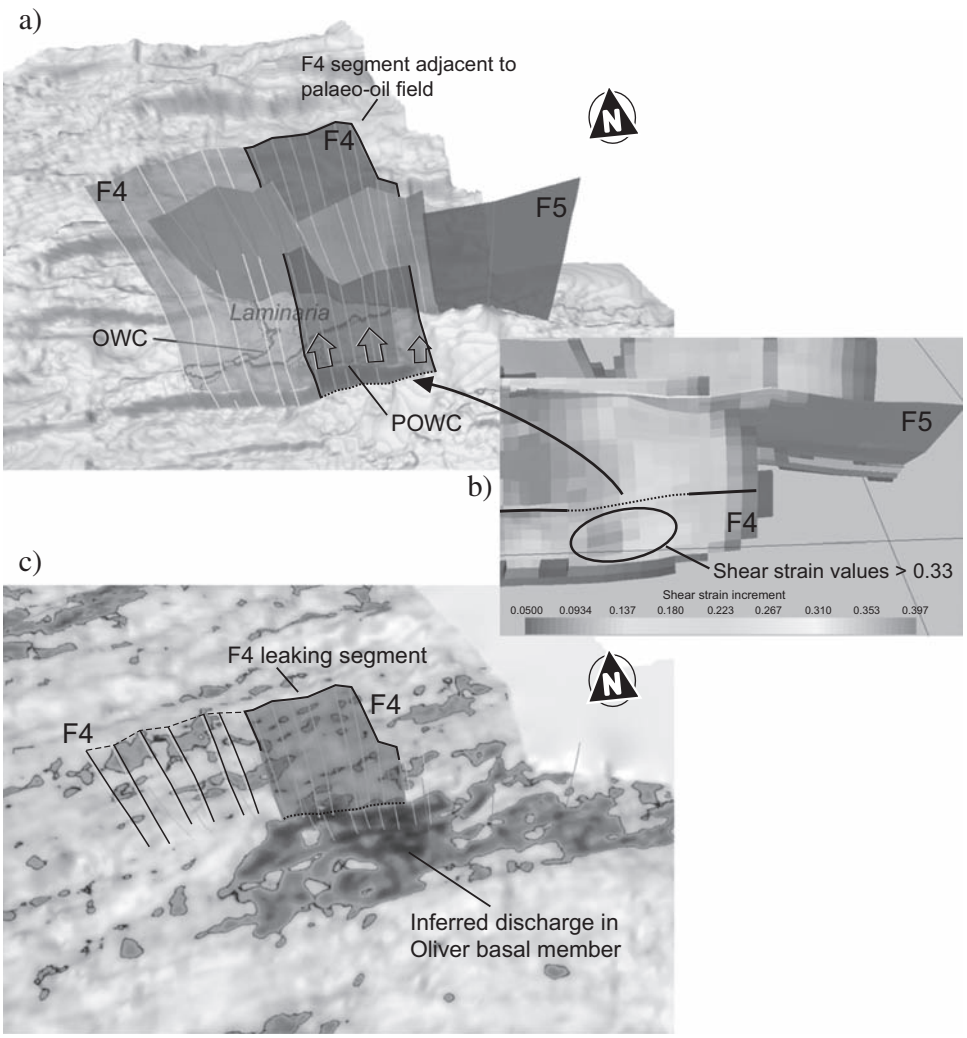

Figure 17. Inferred leakage indicators in the Oliver basal member. (a) Laminaria top reservoir and Laminaria paleofield bounding faults. (b) A 3D detail of the shear-strain distribution at the eastern end of fault F4. (c) Sweetness map in the Oliver basal member, showing the inferred discharge site within the thief zone.

the segment of fault F5 that delimits the breached Capung structure (② in Figure 16).

Discontinuous anomalies are present along the structures that delimit the Corallina field (fault F1, Figure 16). West of the present-day field, a series of anomalies correlates with the distribution of high reactivation strain (Figure 11; ③ in Figure 16). Amplitude and sweetness values grow dim over the present-day oil accumulation where F1 overlaps F2 and accommodates less reactivation strain (Figure 11; ④ in Figure 16). East of the field, anomalies are also visible between two south-dipping synthetic faults, suggesting the presence of an enhanced fluid conduit (⑤ in Figure 16). The overall pattern of anomalies mimics the distribution of the reflectivity on the seabed (Figure 12), with a pocket of relatively low anomalies delimiting the present-day Corallina field.

The reflectivity and sweetness patterns over the Vidalia-Claudea structural trend evolve from west to east, with positive anomalies clustering above the breached Vidalia-1 trap (⑥ in Figure 16). These observations suggest extensive upfault remigration from this closure and average values over the dry (uncharged) Claudea structure.

Interpreted hydrocarbon chimneys

The low-coherency and low-energy near-vertical facies over the Jurassic reservoir horizon typically are associated with faults in the study area, and no clear indication of hydrocarbon chimneys originating directly from the top seal (i.e., away from fault) is observed. However, the recognition of chimneys in the vicinity of faults is often ambiguous because of the presence of fault shadows (Figure 18), shoal shadows, antithetic and synthetic faults, and discontinuous seismic facies associated with the fault zone itself.

A few chimney examples are inferred near the Laminaria and Corallina fields; they represent typical low-coherency and low-energy near-vertical facies located in the hanging-wall compartment (not subject to fault-shadowing effect) and not below a shallow shoal. A restricted chimney

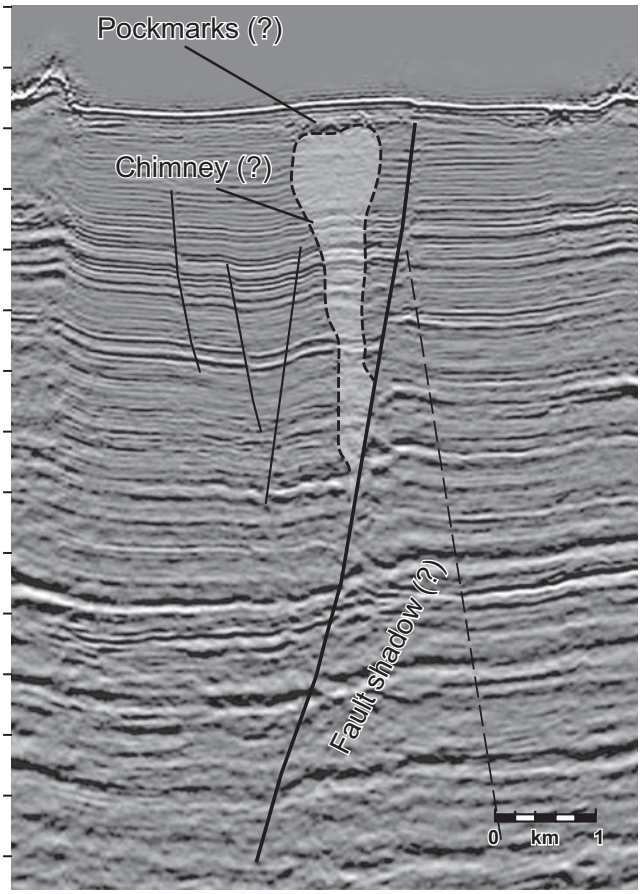

Figure 18. Example of fault shadow creating low-coherency and low-energy near-vertical facies, associated with an inferred chimney in the Nancar trough.

is interpreted as originating from the bend on fault F1 bounding the Corallina paleofield. It represents an approximately 3.5-km-long (~2.2-mile-long) geobody that fully develops where F1 intercepts the base of the Tertiary limestone and extends to the base of the Pliocene (Figure 19b and 19c). However, this geobody is delimited to the north by a small antithetic fault to F1 that could be partly responsible for the chaotic facies.

A chimney is also interpreted at the bend on fault F4, south of the Laminaria present-day field (Figure 19a and 19c). The geobody is restricted to the part of F4 that once bounded the Laminaria paleofield. It is located on the hanging-wall compartment and is delimited to the south by a series of antithetic faults. Although low-coherency and low-energy facies are present in the Cretaceous section, the interpreted chimney seems to develop fully at the base of the Tertiary limestone and extend to at least the base of the Pliocene.

The northern-bounding fault of the Vidalia structure presents the same type of chaotic and low-amplitude facies on the hanging-wall compartment, especially within the Tertiary section. Similar to the Laminaria and Corallina inferred chimneys, the geobody above the breached Vidalia closure is associated with a series of antithetic and synthetic structures to the main fault.

Discussion

Strain distribution and hydrocarbon leakage

The fluid-inclusion data from the Laminaria High clearly indicate the presence of paleo-oil accumulations below the Laminaria and Corallina fields, suggesting that both traps initially were filled beyond the current contacts. Although intense Tertiary reactivation of the Jurassic reservoir faults is the favored mechanism for hydrocarbon remigration (e.g., Shuster et al., 1998; O'Brien et al., 1999; Gartrell and Lisk, 2005; Gartrell et al., 2006; Langhi et al., 2010), loss of hydrocarbon by the effects of water washing has also been proposed (Newell, 1999). However, for water washing to achieve the required level of volume reduction, the traps needed to have been filled initially to spill with gas condensate. This premise contrasts with the available petrographic and geochemical evidence, showing that fluid inclusions trapped in the Laminaria and Corallina fields contain oil rather than gas condensate (George et al., 2004). Furthermore, water washing alone cannot explain the presence of the dry traps that have evidence of significant paleo-oil columns, as is the case for the Laminaria North structure and across the broader northern Bonaparte Basin (i.e., Brincat et al., 2001, 2004; Gartrell et al., 2006). Therefore, the creation of structural permeability during fault reactivation and attendant upfault leakage of hydrocarbons appears to be required to explain the paleo- and present-day oil-column distribution.

The consistency between seismically observed and modeled displacements at 1.5% extension on the fault planes near the Laminaria and Corallina fields (Figure 10) validates the deformation simulation conducted over the study area. Additionally, a high degree of correlation exists between the location of the oil fields (Laminaria and Corallina) and dry structures (Buang, Capung), the leakage indicators (Figures 12, 13, and 16), and the distribution of reactivation strains indicated from the modeling (Figure 11). The distribution of the reactivation shear strain accommodated by fault zones shows the best correlation with hydrocarbon distribution in the study area (Figure 11a and 11b).

The part of fault F1 west of the Corallina field consistently shows seismic anomalies, inferred to reflect fluid migration (Figures 12, 14, 15, and 16), that correlate spatially

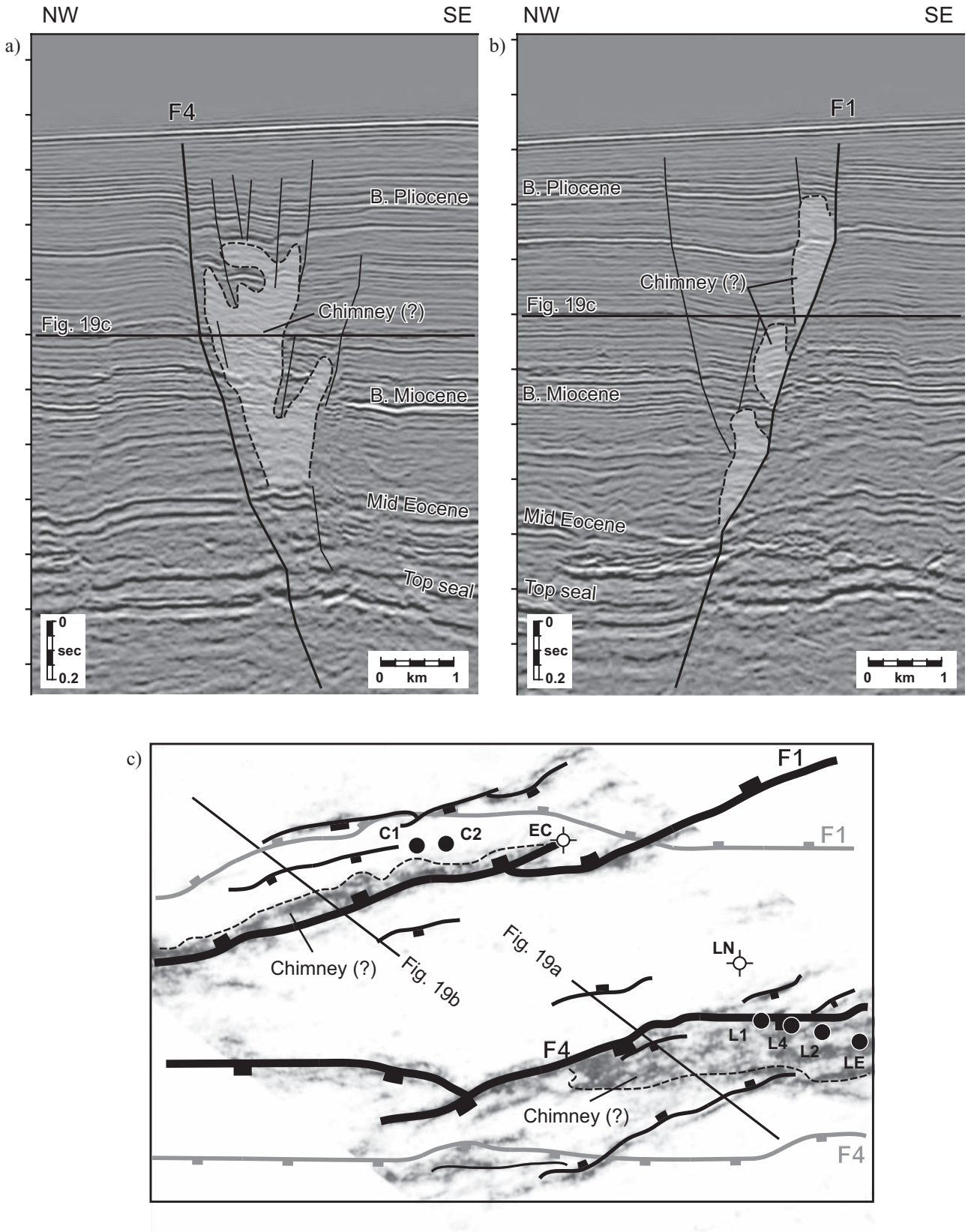

Figure 19. Inferred hydrocarbon chimney. (a) Cross section with an inferred chimney along fault F1. (b) Cross section with an inferred chimney along fault F4. (c) Time slice at 1200 ms, showing the lateral distribution of inferred chimney patterns along faults F1 and F4. Fault traces at the time slice are black; fault traces at top-reservoir level are gray.

with high postrift reactivation shear strain accommodated on this large (~30 km [~18.5 miles]) structure (Figure 11b). Directly west of the field, a jog on F1 is associated with a locus of even higher shear-strain values that matches closely with the position of the present-day OWC (Figure 11a and 11b), suggesting structural permeability enhancement and the development of a probable structurally controlled spill point. The distribution and lateral variation of seismic anomalies at the seafloor (Figure 12) and in the Oliver basal member (Figure 16) as well as the presence of a possible hydrocarbon chimney (Figure 19a and 19b) correlate tightly with the shear-strain locus (Figure 11) and suggest enhancement of fluid circulation on the jog as the cause of hydrocarbon loss from the paleo-oil field.

The extent of the paleo-oil column interpreted at the base of the current accumulation on the Laminaria structure (9 to 22 m [30 to 72 ft]) implies a paleofield delimited to the south by the eastern end of fault F4 (Figure 2), where high reactivation shear strain (Figure 11b) is predicted. This conclusion is consistent with the seismic anomalies noted at the seabed (Figure 12), the Miocene-Pliocene interface (Figure 13), and the Oliver basal member (Figure 16) as well as a possible hydrocarbon chimney (Figure 19c and 19d). These elements support upfault fluid migration near the jog on fault F4, leading to the reduction in size of the Laminaria field.

The present-day Laminaria field is bounded by a splay branch connected with F4 (Figure 2). Because of its short length, this structure was not incorporated into the numerical model. However, the splay is regarded as a low-strain structure due to extensive deformation accommodated by F4 that protects the splay as well as the behavior of the neighboring fault F11 that has a roughly similar size and geometry as the splay and displays a low strain in the model. No seismic anomaly is associated with the splay. The crestal side of the Laminaria field is bounded by the western end of fault F5 (Figure 2) and is modeled to have accommodated low reactivation shear strain (Figure 11b). The distribution of the preserved oil column in the Laminaria field implies that this fault segment has been sealing since the period of charge — an assumption further validated by the lack of seismic anomalies at blind discharge or seafloor expulsion levels.

Much higher shear strain is accommodated by F5 to the east where it does not overlap the neighboring faults F4 and F6 (Figure 11b). This part of the fault bounds the completely breached and now water-wet Capung structure and is associated with seismic anomalies in the Oliver basal member (Figure 16). The weak reflectivity increase reported from the Miocene-Pliocene interface might be from the presence of a carbonate shoal at the seabed, creating velocity effects. The shoal is delimited by F5 (Figure 12) and most likely developed in response to upfault hydrocarbon seepage (e.g., Cowley and O'Brien, 2000; Lavering and Jones, 2002; Rollet et al., 2006).

Paleo-oil columns delineated at Buang and Laminaria North have been breached (Table 1). Although fault F3, bounding the Buang structure, is associated with seismic anomalies at the seabed (Figure 12), the Miocene-Pliocene interface (Figure 13), and the Oliver basal member (Figure 16), few anomalies are associated with F6 over the Laminaria North closure because of the geometry of this north-dipping fault plane (F6) that connects with the south-dipping fault (F4) below the Miocene-Pliocene interface (Figure 4). The deformation model predicts that these structures (F3 and F6) should accommodate less shear strain than neighboring leaking faults (F4, western end of F1; Figure 11b), which initially contradicted the assumption linking reactivation shear strain and structural permeability. However, modeled throws on F3 and F6 appear to be underestimated (Figure 10), which would result in shear strain being underestimated.

Leakage mechanism and controlling parameters

Prior to the Cenozoic reactivation, the upper tips of the main reservoir faults on the Laminaria High were located near the reservoir-seal interface (Gartrell et al., 2006; Ciftci and Langhi, 2010, 2012), only allowing cross-lateral migration between reservoirs units where sand-sand juxtaposition occurs and where no active membrane seal exists in the fault zone. In the numerical model, this observation is honored by keeping fault-zone permeabilities identical to those of host rocks.

For volumetrically significant upfault hydrocarbon leakage to occur, the reservoir bounding the fault must transect the top seal to allow vertical migration to a discharge site (Gartrell et al., 2006). The correlation between the locations of high reactivation shear strain in the model, the extent of the present-day and paleo-oil field, and the distribution of leakage indicators suggest that during reactivation, connection through the top seal may occur preferentially in areas of high shear-strain accommodation on fault planes and due to permeability enhancement in "freshly" damaged fault zones through the top seal. This condition could lead to (1) reservoir-fault upward propagation, (2) dip linkage of reservoir and overlying faults, or (3) the development of a connected fracture network between fault tips (Ciftci and Langhi, 2010, 2012) (Figure 20). Based on the results of deformation experiments on clay soils (Tchalenko, 1970; Bolton et al., 1998; Petley, 1999), Gartrell et al. (2006) propose that the

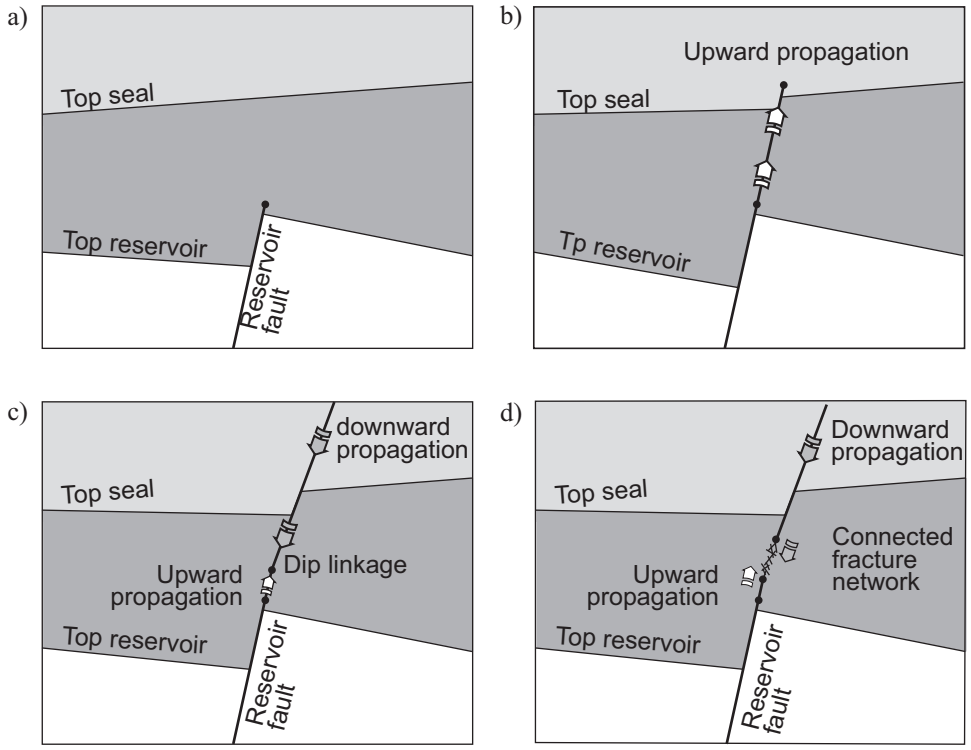

Figure 20. Conceptual model of fault evolution following the Cenozoic extensional reactivation. (a) Prereactivation state. (b) Upward propagation of reservoir fault. The connection across the top seal can be achieved through (c) the dip linkage of reservoir and overlying faults or (d) the development of a connected fracture network between fault tips.

shale and mudstone which form the top seal in the Timor Sea may need sufficient strain to accumulate before ductile deformation gives way to brittle failure and before throughgoing, connected fault zones develop. This process is supported by the modeling results, wherein faults bounding the crestal side of the proven Laminaria and Corallina closures accommodate increased levels of shear and volumetric strains yet retain the present-day accumulations.

Generic numerical geomechanical models (Zhang et al., 2009) and regional studies (e.g., Meyer et al., 2002; Gartrell and List, 2005; Gartrell et al., 2006) demonstrate that the initial fault length provides a primary control on strain distribution between faults in the area. However, with the Cenozoic dominated by extensional deformation approximately normal to the broad strike direction of reservoir faults (Gartrell and Lisk, 2005; Gartrell et al., 2006), additional parameters can significantly impact the distribution of deformation. These include fault spacing, density, and tip arrangements that might modify strain partitioning and locally relieve specific segments of large faults, reducing the reactivation strain below some critical threshold. They also include variation of fault-plane geometry with regard to the regional stress field, which might create shearing-induced dilation loci and develop leak points (Figure 11a–11c).

The interaction of faults most likely impacts structural permeability development, as suggested for the east of the Corallina field, where (1) seafloor reflectivity anomalies are located along a low modeled strain F1 segment, correlating with the development of a triple junction, and where (2) Miocene-Pliocene anomalies along the same segment are associated with overlapping Cenozoic segments, forming a relay zone. Fault intersections have also been shown to be critical sites for hydrocarbon leakage in other parts of the Timor Sea (e.g., Skua field; Gartrell et al., 2004).

Remigration system

The elements presented in this chapter concur with previously published works (O'Brien et al., 1996; Shuster et al., 1998; O'Brien et al., 1999; Gartrell and Lisk, 2005; Gartrell et al., 2006) on Cenozoic tectonics being the driving mechanism behind trap breaching and hydrocarbon seepage in the Laminaria High area and, more generally, across the Timor Sea region. The absence of any clear hydrocarbon chimneys originating directly from the top seal emphasizes the low likelihood of seal failure occurring due to tensile or hydraulic fracturing, as suggested by de Ruig et al. (2000).

Based on fault-growth index mapping on the Laminaria High, Langhi et al. (2011) show that the Cenozoic faulting includes two restricted tectonic phases during the Middle Miocene (16–13 Ma) and the Late Miocene (10–8 Ma) that herald a main period of tectonic activity at the Miocene-Pliocene boundary. This phase is responsible for the regional development of the major Cenozoic fault system in the Laminaria High area. Deformation appears to be ongoing during the Pliocene, with a second tectonic pulse recorded from the growth index at about 3 Ma. Data from Ciftci and Langhi (2010, 2012) suggest that the main Cenozoic deformation stage on the Laminaria High is accommodated by the progressive dip linkage of upward-propagating reservoir faults with downward-propagating newly formed Cenozoic faults. Once enough strain is accommodated on a developing reactivated fault zone (i.e., the zone comprising the lower reservoir fault segment and upper Cenozoic fault segment), connection through the top seal may occur and remigration of hydrocarbons can take place (Figure 20c and 20d).

A rapid establishment of the fault length is inferred for the main period of tectonic activity (Meyer et al., 2002) and suggests the creation of through-going conduits immediately after the Miocene-Pliocene boundary, consistent with the development of seismic anomalies near that stratigraphic level and their interpretation as constructed carbonate buildups. O'Brien et al. (2002) report reef growth initiating in the basal Pliocene south of the study area, near the present-day shelf edge (i.e., near the Buller trap), and they associate these features with hydrocarbon seeps.

The distribution of anomalies at the Miocene-Pliocene boundary along the part of fault F1 that bounds the downdip side of the present-day Corallina trap implies that although this segment accommodated less reactivation shear strain and defines a shielded area, it might still have initially experienced some degree of leakage. Thus, at the time of maximum fault activity and shear-strain accommodation (Miocene-Pliocene), a connection across the top seal might have initially developed between the reservoir and the Cenozoic fault segments. However, the absence of a seismic-leakage indicator at that location in the Oliver basal member or at the seabed and the presence of a present-day oil column against this fault segment imply that such a "low shear-strain connection" was not sustained through time.

Fault zones that accommodated sufficient shear strain to develop a well-connected pathway across the top seal are typically characterized by an upper tip located between the Miocene-Pliocene boundary and the present-day seabed. This observation implies that these structures intercept the entire Cretaceous-Tertiary stratigraphic column, including units with good reservoir properties where leaking hydrocarbon can be stored temporarily (thief zones). Over the study area, variations of seismic facies interpreted as indications of fluid circulation along faults are probably present in the Grebe (Eocene) Sandstone formations and are intercalated into the Late Cretaceous-Tertiary carbonate platform. However, low S/N compromises the accurate assessment of these anomalies. The base Miocene Oliver basal member, formed of sandstone or calcarenite, presents clear seismic anomalies controlled by the structural network and interpreted as evidence of fluid discharge. Lateral lithological variations due to sandstone bypass can affect the distribution of leakage anomalies; however, on the Laminaria High, anomalies are also recognized where the Oliver basal member is formed by calcarenites. The areal distribution of the anomalies clearly exceeds the areal location of the late Jurassic closures (Figures 12, 13, and 16), suggesting that the hydrocarbon leaking upfault originates from trapped oil accumulations and is fed by migration routes along the main structural trends.

Based on the elements presented here, the favored model for hydrocarbon remigration includes an initial Miocene-Pliocene phase of leakage following the development of pathways across the top seal due to shear-strain accommodation, leading to reservoir-level fault reactivation, linkage with Cenozoic faults, and the development of the conduits to the base Pliocene seafloor (Figure 21). Although part of the leaking hydrocarbon remigrated upfault to the free surface, promoting authigenic carbonate hardgrounds and localized carbonate reef development, another part was discharged into thief zones intercepted by these conductive structures (Figure 21). During this main phase of structural reactivation, hydrocarbon chimneys might have developed (Figures 18 and 19) at specific locations where shear strain concentrated (e.g., fault jogs). The development of such features appears to have been dependent on the development of secondary Cenozoic structures, antithetic and synthetic to the main fault plane.

Ongoing leakage probably occurred during most of the Pliocene, whereas deformation continues to be accommodated by reservoir faults and Cenozoic faults (Figure 21). Within the Pliocene, buried thief zones could be charged and chimneys further developed. Deformation decreased significantly during the Pleistocene (Langhi et al., 2011), although most of the major faults are still active, as shown by offsets near the seafloor. The seismic anomalies recorded from that level suggest that at least a residual "soft-bleed" leakage (George et al., 2004) occurred during the Pleistocene from fault segments that experienced most of the shear deformation during the Cenozoic (Figure 21).

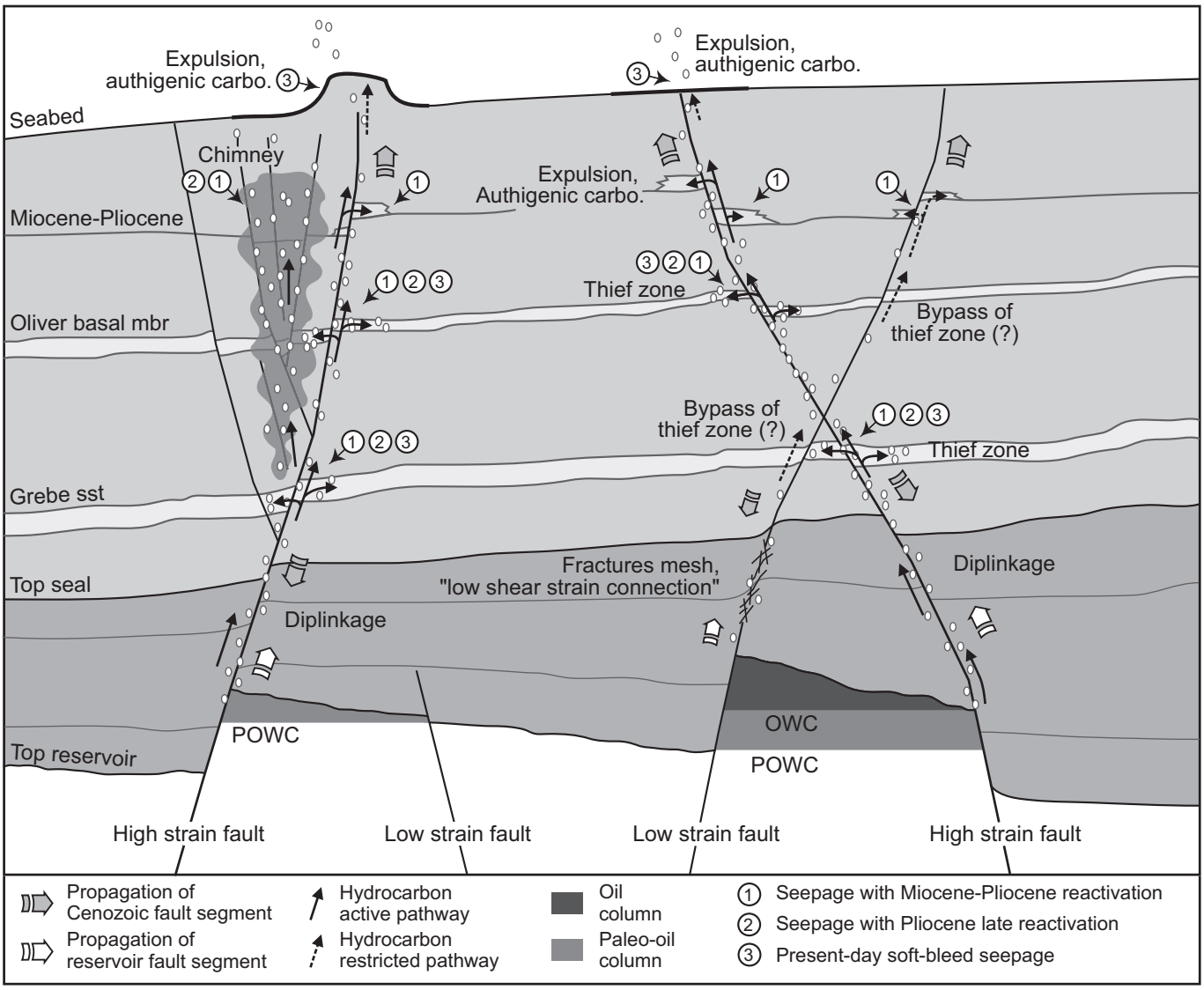

Figure 21. Conceptual model for postreactivation remigration on the Laminaria High. For each critical location, the timing of possible seepage is shown with ① seepage coeval with the Miocene-Pliocene maximum reactivation event, ② seepage ongoing during the Pliocene late reactivation stage, and ③ present-day soft-bleed seepage resulting from residual structural permeability.

Conclusions

Observations from multiple data sets and a range of analytical techniques have been integrated to form a robust understanding of the processes that have controlled hydrocarbon leakage and preservation patterns on the Laminaria High region of the Timor Sea. There are seven main conclusions of our work.

First, this case study demonstrates that numerical simulations involving 3D coupled mechanical and fluid-flow numerical models can be used to simulate the relationship between deformation and fluid migration along naturally complex fault systems that deform under an extensional reactivation setting. In the Laminaria High area, the model accommodates the distribution of a suite of leakage observations and can be used to predict upfault hydrocarbon remigration pathways with increased confidence.

Second, the results of the work consolidate previous models (Gartrell and Lisk, 2005; Gartrell et al., 2006), relating trap integrity in the Laminaria High and greater Timor Sea region to the heterogeneous distribution of shear strain within a system of overlapping faults.

Third, the heterogeneous distribution of reactivational shear strain on fault zones provides the first-order control on upfault remigration associated with the breaching of traps. Once sufficient shear strain is accommodated on a

fault zone comprising the lower reactivated reservoir-fault segment and upper newly formed Cenozoic fault segment, ductile deformation yielding to brittle failure and connection through the top seal may occur, leading to the development of an open permeable pathway.

Fourth, fault size (strike length and height) is the first-order control for the distribution of reactivation shear strain. However, the fault spacing, density, and arrangements at the tip of the fault all produce an impact on strain partitioning that might locally help reduce the reactivation strain and create shielded areas less prone to upfault remigration. Fault jogs are present at reservoir level due to lateral fault-segment growth and linkage; during the Cenozoic reactivation phase, these features concentrated shear and dilatational strain and hence may form preferential leakage pathways.

Fifth, charge-history reconstruction constrained by fluid-inclusion data together with coupled modeling outcomes show that structures accommodating low shear strain during the Cenozoic are more likely to retain hydrocarbon accumulations than structures accommodating high shear strain. However, seismic interpretation of leakage indicators suggests that even shielded fault segments holding a current hydrocarbon column might have experienced some leakage at the peak of the reactivation phase at the Miocene-Pliocene boundary.

Sixth, a conceptual model of the local remigration system suggests that most of the leakage occurred directly after the Miocene-Pliocene boundary on fault planes accommodating higher values of shear strain, resulting in upfault hydrocarbon remigration with expulsion at the seafloor as well as discharge into buried thief zones.

Finally, although we propose that episodes of dynamic leakage occurred during most of the Pliocene, the deformation that continues to be accommodated by fault zones today is linked less clearly. Nevertheless, seismic evidence near the present-day seafloor suggests that a residual "soft-bleed" leakage process might still be occurring.

References

AGSO North West Shelf Study Group, 1994, Deep reflections on the North West Shelf: Changing perceptions of basin formation: Proceedings of the 1st Petroleum Exploration Society of Australia Symposium, 63–76.

Aminzadeh, F., D. Connolly, R. Heggland, and P. deGroot, 2002, Geohazard detection and other applications of chimney cubes: The Leading Edge, **21**, 681–685, http://dx.doi.org/10.1190/1.1497324.

Anderson, R. N., P. Flemings, S. Losh, J. Austin, and R. Woodhams, 1994, Gulf of Mexico growth fault drilled, seen as oil, gas migration pathway: Oil & Gas Journal, **94**, no. 23, 97–104.

Bailey, W., P. M. Shannon, J. J. Walsh, and V. Unnithan, 2003, The spatial distributions of faults and deep sea carbonate mounds in the Porcupine Basin, offshore Ireland: Marine and Petroleum Geology, **20**, 509–522, http://dx.doi.org/10.1016/S0264-8172(03)00079-5.

Baillie, P. W., C. M Powell, Z. X. Li, and A. M. Ryall, 1994, The tectonic framework of Western Australia's Neoproterozoic to Recent sedimentary basins: Proceedings of the 1st Petroleum Exploration Society of Australia Symposium, 45–62.

Barnes, A. E., 2007, Redundant and useless seismic attributes: Geophysics, **72**, no. 3, 33–38, http://dx.doi.org/10.1190/1.2716717.

Barton, C. A., M. D. Zoback, and D. Moos, 1995, Fluid flow along potentially active faults in crystalline rock: Geology, **23**, 683–686, http://dx.doi.org/10.1130/0091-7613(1995)023<0683:FFAPAF>2.3CO;2.

Bear, J., and A. Verruijt, 1987, Modelling groundwater flow and pollution: D. Reidel.

Bjørlykke, K., K. Høeg, J. I. Faleide, and J. Jahren, 2005,When do faults in sedimentary basins leak? Stress and deformation in sedimentary basins — Examples from the North Sea and Haltenbanken, offshore Norway: AAPG Bulletin, **89**, 1019–1031, doi:10.1306/04010504118.

BHP, 1996, Laminaria East-1 internal well completion report.

Bolton, A. J., A. J. Maltman, and M. B. Clennell, 1998, The importance of overpressure timing and permeability evolution in fine-grained sediments undergoing shear: Journal of Structural Geology, **20**, 1013–1022, http://dx.doi.org/10.1016/S0191-8141(98)00030-3.

Bradley, D. C., and W. S. F. Kidd, 1991, Flexural extension of the upper continental crust in collisional foredeeps: Geological Society of America Bulletin, **59**, 1416–1438, http://dx.doi.org/10.1130/0016-7606(1991)103<1416:FEOTUC>2.3.CO;2.

Brincat, M. P., W. Bailey, S. M. Mildren, and M. Lisk, 2004, Integrated integrity analysis in a reactivated setting: Examples from the northern Bonaparte Basin, Australia: EAGE Faults and Top Seals Conference Proceedings, 12.

Brincat, M. P., and P. J. Eadington, 1998, Hydrocarbon petrography of the Laminaria formation at Vidalia-1, Bonaparte Basin: Australian Petroleum Cooperative Research Centre (APCRC) Confidential Report 348.

Brincat, M., A. Gartrell, M. Lisk, W. Bailey, L. Johnson, and D. Dewhurst, 2006, An integrated evaluation of hydrocarbon charge and retention at the Griffin, Chinook, and Scindian oil and gas fields, Barrow Subbasin,

North West Shelf, Australia: AAPG Bulletin, **90**, 1359–1380, doi:10.1306/02210605103.

Brincat, M. P., G. W. O'Brien, M. Lisk, M. de Ruig, and S. C. George, 2001, Hydrocarbon charge history of the northern Londonderry High: Implications for trap integrity and future prospectivity: Australian Petroleum Production and Exploration Association (APPEA) Journal, **41**, 483–496.

Caine, J. S., J. P. Evans, and C. B. Forster, 1996, Fault zone architecture and permeability structure: Geology, **24**, 1025–1028, doi:10.1130/0091-7613(1996)024<1025:FZAAPS>2.3.CO;2.

Castillo, D. A., R. R., Hillis, K. Asquith, and M. Fischer, 1998, State of stress in the Timor Sea area, based on deep wellbore observations and frictional failure criteria: Application to fault-trap integrity: Proceedings of the 2nd Petroleum Exploration Society of Australia Symposium, 325–341.

Charlton, T. R., 2000, Tertiary evolution of the Eastern Indonesia collision complex: Journal of Asian Earth Sciences, **18**, 603–631, doi:10.1016/S1367-9120(99)00049-8.

Charlton, T. R., A. J. Barber, and S. T Barkham, 1991, The structural evolution of the Timor collision complex, eastern Indonesia: Journal of Structural Geology, **13**, 489–500, doi:10.1016/0191-8141(91)90039-L.

Ciftci, B., and L. Langhi, 2010, Time-transgressive fault evolution and its impact on trap integrity: Timor Sea examples: Australian Petroleum Production and Exploration Association (APPEA) Conference, Extended Abstracts.

Ciftci, B., and L. Langhi, 2012, Evolution of the hourglass structures in the Laminaria High, Timor Sea: Implications for hydrocarbon traps: Journal of Structural Geology, **36**, 55–70, doi:10.1016/j.jsg.2011.12.006.

Cowley, R., and G. W. O'Brien, 2000, Identification and interpretation of leaking hydrocarbons using seismic data: A comparative montage of examples from the major fields in Australia's North West Shelf and Gippsland Basin: Australian Petroleum Production and Exploration Association (APPEA) Journal, **40**, 121–150.

Cundall, P., and M. Board, 1988, A microcomputer program for modelling large-strain plasticity problems: Numerical Methods in Geomechanics, **6**, 2101–2108.

Dando, P. R., M. C. Austen, R. J. Burke, M. A. Kendall, M. C. Kennicutt, A. G. Judd, D. C. Moore, S. C. M. O'Hara, R. Schmaljohann, and A. J. Southward, 1991, Ecology of a North Sea pockmark with an active methane seep: Marine Ecology Progress Series, **70**, 49–63.

de Ruig, M. J., M. Trupp, D. J. Bishop, D. Kuek, and D. A. Castillo, 2000, Fault architecture and the mechanics of fault reactivation in the Nancar trough/ Laminaria area of the Timor Sea, northern Australia: Australian Petroleum Production and Exploration Association (APPEA) Journal, **40**, 174–193.

Dutkiewicz, A., and P. J. Eadington, 1997, Hydrocarbon charge and fluid migration history of the Callovian Laminaria Formation in Alaira-1, Laminaria High: CSIRO Confidential Report 297.

Dutkiewicz, A., M. Lisk, and P. J. Eadington, 1997, Hydrocarbon charge and fluid migration history of Jurassic sandstones in WA-260-P: Australian Petroleum Cooperative Research Centre (APCRC) Confidential Report 300.

Eadington, P. J., M. Lisk, and F. W. Krieger, 1996, Identifying oil well sites: U. S. patent 5,543,616, www.patentstorm.us/patents/5543616.html.

Edwards, H., J. Crosby, N. David, C. Loader, and S. Westlake, 2005, Australian Megasurveys — The key to new discoveries in maturing areas?: Australian Petroleum Production and Exploration Association (APPEA) Journal, **45**, 407–420.

Færseth, R. B., E. Johnsen, and S. Sperrevik, 2007, Methodology for risking fault seal capacity: Implications of fault zone architecture: AAPG Bulletin, **91**, 1231–1246, doi:10.1306/03080706051.

Fisher, Q. J., M. Casey, X. Harris, and R. J. Knipe, 2003, Fluid-flow properties of faults in sandstones: The importance of temperature history: Geology, **31**, 965–968, doi.org/10.1130/G19823.1.

Fisher, Q. J., and R. J. Knipe, 2001, The permeability of faults within siliciclastic petroleum reservoirs of the North Sea and Norwegian continental shelf: Marine and Petroleum Geology, **18**, 1063–1081, doi:10.1016/S0264-8172(01)00042-3.

Gartrell, A., W. R. Bailey, and M. Brincat, 2006, A new model for assessing trap integrity and oil preservation risks associated with postrift fault reactivation in the Timor Sea: AAPG Bulletin, **90**, 1921–1944, doi:10.1306/06200605195.

Gartrell, A. P., and M. Lisk, 2005, Potential new method for paleostress estimation by combining 3D fault restoration and fault slip inversion techniques: First test on the Skua field, Timor Sea, *in* P. Boult and J. K. Kaldi, eds., Evaluating fault and cap rock seals: AAPG, 23–36.

Gartrell, A., Y. Zhang, M. Lisk, and D. Dewhurst, 2004, Fault intersections as critical hydrocarbon leakage zones: Integrated field study and numerical modeling of an example from the Timor Sea, Australia: Marine and Petroleum Geology, **21**, 1165–1179.

George, S. C., T. E. Ruble, H. Volk, M. Lisk, M. P. Brincat, A. Dutkiewicz, and M. Ahmed, 2004, Comparing the geochemical composition of fluid inclusion and crude

oils from wells on the Laminaria High, Timor Sea: Proceedings of the Timor Sea Symposium, 203–230.

Giroldi, L., F. Alegria, L. Gochioco, and P. Cunningham, 2005, Using spectral decomposition to identify and characterize glacial valleys and fluvial channels within the Carboniferous section in Bolivia: The Leading Edge, **24**, 1152–1159, doi:10.1190/1.2135127.

Halliday, E. J., J. V. Barrie, N. R. Chapman, and K. M. M. Rohr, 2008, Structurally controlled hydrocarbon seeps on a glaciated continental margin, Hecate Strait, offshore British Columbia: Marine Geology, **252**, 193–206, doi:10.1016/j.margeo.2008.04.009.

Haney, M. M., R. Snieder, J. Sheiman, and S. Losh, 2005, A moving fluid pulse in a fault zone: Nature, **437**, no. 46, doi:10.1038/4370461.

Harrowfield, M., J. Cunneen, M. Keep, and W. Crowe, 2003, Early-stage orogenesis in the Timor Sea region, NW Australia: Journal of the Geological Society of London, **160**, 991–1002.

Heggland, R., 2005, Using gas chimneys in seal integrity analysis: A discussion based on case histories, *in* P. Boult and J. K. Kaldi, eds., Evaluating fault and cap rock seals: AAPG, 237–245.

Hovland, M., P. F. Croker, and M. Martin, 1994, Fault-associated seabed mounds (carbonate knolls?) off western Ireland and north-west Australia: Marine and Petroleum Geology, **11**, 232–246, doi:10.1016/0264-8172(94)90099-X.

Hovland, M., and A. G. Judd, 1988, Seabed pockmarks and seepages: Impact on geology, biology and the marine environment: Graham and Trotman.

Hovland, M., M. Talbot, S. Olaussen, and L. Aasberg, 1985, Recently formed methane-derived carbonates from the North Sea floor, *in* B. M. Thomas, ed., Petroleum geochemistry in exploration of the Norwegian Shelf: Norwegian Petroleum Society, 236–266.

Isaksen, G. H., R. J. Pottorf, and A. I. Jenssen, 1998, Correlation of fluid inclusions and reservoired oils to infer trap fill history in the South Viking Graben, North Sea: Petroleum Geoscience, **4**, 41–55, doi:10.1144/petgeo.4.1.41.

Itasca, 2005, Fast Lagrangian analysis of Continua in 3 dimensions — User manual, version 3.1: Itasca Consulting Group, Inc.

Judd, A. G., M. Hovland, and A. M. Davis, 1992, The evidence of shallow gas in marine sediments: Continental Shelf Research, **12**, 1081–1095, doi:10.1016/0278-4343(92)90070-Z.

Karlsen, D. A., T. Nedkvitne, S. R. Larter, and K. Bjørlykke, 1993, Hydrocarbon composition of authigenic inclusions: Application to elucidation of petroleum reservoir filling history: Geochimica et Cosmochimica Acta, **57**, 3641–3659, doi:10.1016/0016-7037(93)90146-N.

Keep, M., M. Clough and L. Langhi, 2002, Neogene tectonic and structural evolution of the Timor Sea region, NW Australia: Proceedings of the 3rd Petroleum Exploration Society of Australia Symposium, 341–353.

Kennard, J. M., I. Deighton, D. S. Edward, J. B. Colwell, G. W. O'Brien, and C. J. Boreham, 1999, Thermal history modelling and transient heat pulses: New insights into hydrocarbon expulsion and 'hot flushes' in the Vulcan sub-basin, Timor Sea: Australian Petroleum Production and Exploration Association (APPEA) Journal, **39**, 177–207.

Labutis, V. R., A. D. Ruddock, and A. P. Calcraft, 1998, Stratigraphy of the Sahul platform: Australian Petroleum Production and Exploration Association (APPEA) Journal, **38**, 115–136.

Langhi, L., 2009, Spectral decomposition of 3D seismic megasurvey for definition of hydrocarbon remigration systems and prediction of traps integrity: Australian Society of Exploration Geophysicists (ASEG) Conference, Extended Abstracts.

Langhi, L., and G. D. Borel, 2008, Reverse structures in accommodation zone and early compartmentalization of extensional system, Laminaria high (NW shelf, Australia): Marine and Petroleum Geology, **25**, 791–803, doi:10.1016/j.marpetgeo.2008.04.007.

Langhi, L., B. Ciftci, and G. Borel, 2011, Impact of lithospheric flexure on the evolution of shallow faults in the Timor foreland basin: Marine and Petroleum Geology, **284**, 40–54.

Langhi, L., Y. Zhang, A. Gartrell, J. R. Underschultz, and D. N. Dewhurst, 2010, Evaluating hydrocarbon trap integrity during fault reactivation using geomechanical three-dimensional modelling: An example from the Timor Sea, Australia: AAPG Bulletin, **94**, 567–591, doi:10.1306/10130909046.

Lavering, I., and A. Jones, 2002, Carbonate shoals and hydrocarbons in the western Timor Sea: PESA News, **55**, 40–42.

Ligtenberg, J. H., 2003, Unravelling the petroleum system by enhancing fluid migration paths in seismic data using a neural network based pattern recognition technique: Geofluids, **3**, 255–261, doi:10.1046/j.1468-8123.2003.00072.x.

Ligtenberg, J. H., 2005, Detection of fluid migration pathways in seismic data: Implications for fault seal analysis: Basin Research, **17**, 141–153, doi:10.1111/j.1365-2117.2005.00258.x.

Lisk, M., M. P. Brincat, P. J. Eadington, and G. W. O'Brien, 1998, Hydrocarbon charge in the Vulcan Sub-basin:

Proceedings of the 2nd Petroleum Exploration Society of Australia Symposium, 287–303.

Lisk, M., and P. J. Eadington, 1994, Oil migration in the Cartier trough, Vulcan Sub-basin: Proceedings of the West Australian Basins Symposium, 301–312.

Lisk, M., S. C. George, R. E. Summons, R. A. Quezada, and G. W. O'Brien, 1996, Mapping hydrocarbon charge histories: Detailed characterisation of the South Pepper oil field, Carnarvon Basin: Australian Petroleum Production and Exploration Association (APPEA) Journal, **36**, 445–464.

Lisk, M., D. Hall, J. Ostby, and M. P. Brincat, 2001, Addressing the oil migration risks in the Great Australian Bight: PESA Eastern Australasian Basins Symposium, 553–562.

Lisk, M., G. W. O'Brien, and P. J. Eadington, 2002, Quantitative evaluation of the oil-leg potential in the Oliver gas field, Timor Sea, Australia: AAPG Bulletin, **86**, 1531–1542.

Longley, I. M., C. Buessenschuett, L. Clydsdale, C. J. Cubitt, R. C. Davis, M. K. Johnson, N. M. Marshall, A. P. Murray, R. Somerville, T. B. Spry, and N. B. Thompson, 2002, The North West Shelf of Australia: A Woodside perspective: Proceedings of the 3rd Petroleum Exploration Society of Australia Symposium, 27–88.

Lorenzo, J., G. W. O'Brien, J. Stewart, and K. Tandon, 1998, Inelastic yielding and forebulge shape across a modern foreland basin: North West Shelf of Australia, Timor Sea: Geophysical Research Letters, **25**, 1455–1458, doi:10.1029/98GL01012.

Losh, 1998, Oil migration in a major growth fault: Structural analysis of the Pathfinder core, South Eugene Island block 330, offshore Louisiana: AAPG Bulletin, **82**, 1694–1710.

Losh, S., L. Eglinton, M. Schoell, and J. Wood, 1999, Vertical and lateral fluid flow related to a large growth fault, South Eugene Island block 330 field, onshore Louisiana: AAPG Bulletin, **83**, 244–276.

Marchal, D., M. Guiraud, and T. Rives, 2003, Geometric and morphologic evolution of normal fault planes and traces from 2D to 4D data: Journal of Structural Geology, **25**, 135–158, doi:10.1016/S0191-8141(02)00011-1.

McLellan, J. G., N. H. S. Oliver, and P. M. Schaubs, 2004, Fluid flow in extensional environments: Numerical modelling with an application to Hamersley iron ores: Journal of Structural Geology, **26**, 1157–1171, doi:10.1016/j.jsg.2003.11.015.

Meldahl, P., R. Heggland, A. Bril, and P. de Groot, 2001, Identifying fault and gas chimneys using multi-attributes and neural networks: The Leading Edge, **20**, 474–482, doi:10.1190/1.1438976.

Meyer, V., A. Nicol, C. Childs, J. J. Walsh, and J. Watterson, 2002, Progressive localisation of strain during the evolution of a normal fault population: Journal of Structural Geology, **24**, 1215–1231, doi:10.1016/S0191-8141(01)00104-3.

Muir-Wood, R., and G. C. P. King, 1993, Hydrological signatures of earthquake strain: Journal of Geophysical Research, **98**, no. B12, 22035–22068, doi:10.1029/93JB02219.

Newell, N.A., 1999, Water-washing in the northern Bonaparte Basin: Australian Petroleum Production and Exploration Association (APPEA) Journal, **39**, 227–247.

O'Brien, G. W., M. A. Etheridge, J. B. Willcox, M. Morse, P. Symonds, C. Norman, and D. J. Needham, 1993, The structural architecture of the Timor Sea, northwestern Australia; Implications for basin development and hydrocarbon exploration: Australian Petroleum Exploration Association (APEA) Journal, **33**, 258–278.

O'Brien G. W., K. Glenn, G. Lawrence, A. K. Williams, M. Webster, S. Burns, and R. Cowley, 2002, Influence of hydrocarbon migration and seepage on benthic communities in the Timor Sea, Australia: Australian Petroleum Production and Exploration Association (APPEA) Journal, **42**, 225–240.

O'Brien, G. W., R. Higgins, P. Symonds, P. Quaife, J. Colwell, and J. Blevin, 1996, Basement control on the development of extensional systems in Australia's Timor Sea: An example of hybrid hard linked/soft linked faulting?: Australian Petroleum Production and Exploration Association (APPEA) Journal, **36**, 161–200.

O'Brien, G. W., M. Lisk, I. R. Duddy, J. Hamilton, P. Woods, and R. Cowley, 1999, Plate convergence, foreland development and fault reactivation; Primary controls on brine migration, thermal histories and trap breach in the Timor Sea, Australia: Marine and Petroleum Geology, **16**, 533–560, doi:10.1016/S0264-8172(98)00070-1.

O'Brien, G. W., and E. P. Woods, 1995, Hydrocarbon-related diagenetic zones (HRDZs) in the Vulcan sub-basin, Timor Sea: Recognition and exploration implications: Australian Petroleum Exploration Association (APEA) Journal, **35**, 220–252.

Ord, A., 1991, Deformation of rock: A pressure-sensitive, dilatant material: Pure and Applied Geophysics, **137**, 337–366, doi:10.1007/BF00879039.

Ord, A., and N. H. S. Oliver, 1997, Mechanical controls on fluid flow during regional metamorphism: Some numerical models: Journal of Metamorphic Geology, **15**, 345–359, doi:10.1111/j.1525-1314.1997.00030.x.

Partyka, G., J. Gridley, and J. Lopez, 1999, Interpretational applications of spectral decomposition in reservoir

characterization: The Leading Edge, **18**, 353–360, doi:10.1190/1.1438295.

Pattillo, J., and P. J. Nicholls, 1990, A tectono-stratigraphic framework for the Vulcan Graben, Timor Sea region: Australian Petroleum Production and Exploration Association (APPEA) Journal, **30**, 27–51.

Petley, D. N., 1999, Failure envelopes of mudrocks at high confining pressures, *in* A. C. Aplin, A. J. Fleet, and J. H. S. Macquaker, eds., Muds and mudstones: Physical and fluid flow properties: Geological Society (London) Special Publication 158, 61– 71.

Revil, A., and L. M. Cathles III, 2002, Fluid transport by solitary waves along growing faults: A field example from the South Eugene Island Basin, Gulf of Mexico: Earth and Planetary Science Letters, **202**, no. 2, 321–335, doi:10.1016/S0012-821X(02)00784-7.

Roberts, H., B. Hardage, W. Shedd, and J. Hunt, 2006, Seafloor reflectivity — An important seismic property for interpreting fluid/gas expulsion geology and the presence of gas hydrate: The Leading Edge, **25**, 620–628, doi:10.1190/1.2202667.

Rollet, N., G. A Logan, J. M. Kennard, G. W. O'Brien, A. T. Jones, and M. Sexton, 2006, Characterisation and correlation of active hydrocarbon seepage using geophysical data sets; An example from the tropical, carbonate Yampi Shelf, Northwest Australia: Marine and Petroleum Geology, **2**, no. 2, 145–164, doi:10.1016/j.marpetgeo.2005.10.002.

Shuster, M. W., S. Eaton, L. L. Wakefield, and H. J. Kloosterman, 1998, Neogene tectonics, Greater Timor Sea, offshore Australia: Implications for trap risk: Australian Petroleum Production and Exploration Association (APPEA) Journal, **38**, 351–379.

Sibson, R. H., 1992, Fault-valve behavior and the hydrostatic-lithostatic fluid pressure interface: Earth-Science Reviews, **32**, no. 1-2, 141–144, doi:10.1016/0012-8252(92)90019-P.

Sibson, R. H., 1996, Structural permeability of fluid-driven fault-fracture meshes: Journal of Structural Geology, **18**, 1031–1042, doi:10.1016/0191-8141(96)00032-6.

Sleep, N. H., and M. L. Blanpied, 1992, Creep, compaction and the weak rheology of major faults: Nature, **359**, 687–692, doi:10.1038/359687a0.

Smith, G. C., L. A. Tilbury, A. Chatfield, P. Senycia, and N. Thompson, 1996, Laminaria — A new Timor Sea discovery: Australian Petroleum Production and Exploration Association (APPEA) Journal, **36**, 12–28.

Strayer, L. M., P. J. Hudleston, and L. J. Lorig, 2001, A numerical model of deformation and fluid-flow in an evolving thrust wedge: Tectonophysics, **335**, no. 1-2, 121–145, doi:10.1016/S0040-1951(01)00052-X.

Tchalenko, J. S., 1970, Similarities between shear zones of different magnitudes: GSA Bulletin, **81**, 1625–1640, doi:10.1130/0016-7606(1970)81[1625:SBSZOD]2.0.CO;2.

Underschultz, J. R., 2005, Pressure distribution in a reservoir affected by capillarity and hydrodynamic drive: Griffin field, North West Shelf, Australia: Geofluids, **5**, no. 3, 221–235, doi:10.1111/j.1468-8123.2005. 00112.x.

Underschultz, J. R., 2007, Hydrodynamics and membrane seal capacity: Geofluids, **7**, no. 2, 148–158, doi:10.1111/j.1468-8123.2007.00170.x.

Underschultz, J. R., C. J. Otto, and R. Bartlett, 2005, Formation fluids in faulted aquifers; Examples from the foothills of western Canada and the North West Shelf of Australia, *in* P. Boult and J. Kaldi, eds., Evaluating fault and cap rock seals: AAPG, 247–260.

Vermeer, P. A., and R. de Borst, 1984, Non-associated plasticity for soils, concrete and rocks: Heron, **29**, 1–64.

Whittam, D. B., M. S. Norvick, and C. L. McIntyre, 1996, Mesozoic and Cenozoic tectonostratigraphy of western Zoca and adjacent areas: Australian Petroleum Production and Exploration Association (APPEA) Journal, **36**, 209–231.

Wilkins, S. J., and S. J. Naruk, 2007, Quantitative analysis of slip-induced dilation with application to fault seal: AAPG Bulletin, **91**, 97–113, doi:10.1306/08010605177.

Woodside Offshore Petroleum Pty. Ltd., 1997, Laminaria-4 internal well completion report.

Worden, R. H., and S. Morad, 2000, Quartz cementation in oil field sandstones: A review of the key controversies: International Association of Sedimentologists Special Publication 29, 1–20.

Zhang, S., and S. F. Cox, 2000, Enhancement of fluid permeability during shear deformation of a synthetic mud: Journal of Structural Geology, **22**, 1385–1393, doi:10.1016/S0191-8141(00)00065-1.

Zhang, Y., A. Gartrell, J. R. Underschultz, and D. N. Dewhurst, 2009, Numerical modelling of strain localisation and fluid flow during extensional fault reactivation: Implications for hydrocarbon preservation: Journal of Structural Geology, **31**, 315–327, doi:10.1016/j.jsg.2008.11.006.